

Ancient TL

A periodical devoted to Luminescence and ESR dating

Department of Geography and Earth Sciences, Aberystwyth
University, Ceredigion SY23 3DB, United Kingdom

Volume 31 No.2

December 2013

R package *numOSL*: numeric routines for optically stimulated luminescence

J. Peng, Z. B. Dong, F.Q. Han, H. Long, X. J. Liu _____ 41

Optimising the reproducibility of measurements of the post-IR IRSL signal from single-grains of K-feldspar for dating

R.K. Smedley, G. A. T. Duller _____ 49

Thesis abstracts

Z. Gong _____ 59

J.A. Durcan _____ 59

A. Medialdea _____ 60

Y. Chen _____ 61

C. Leighton _____ 61

Bibliography _____ 63

Announcements

LumiDoz 8 International Conference on Luminescence and ESR
Dosimetry, Ankara _____ 73

ISSN 0735-1348

Ancient TL

Started by the late David Zimmerman in 1977

EDITOR

G.A.T. Duller, Department of Geography and Earth Sciences, Aberystwyth University, Ceredigion SY23 3DB, United Kingdom (ggd@aber.ac.uk)

EDITORIAL BOARD

I.K. Bailiff, Luminescence Dosimetry Laboratory, Dawson Building, University of Durham, South Road, Durham DH1 3LE, United Kingdom (ian.bailiff@durham.ac.uk)

R.DeWitt, Department of Physics, East Carolina University, Howell Science Complex, 1000 E. 5th Street Greenville, NC 27858, USA (dewittr@ecu.edu)

S.H. Li, Department of Earth Sciences, The University of Hong Kong, Hong Kong, China (shli@hku.hk)

R.G. Roberts, School of Geosciences, University of Wollongong, Wollongong, NSW 2522, Australia (rgrob@uow.edu.au)

REVIEWERS PANEL

R.M. Bailey, Oxford University Centre for the Environment, Dyson Perrins Building, South Parks Road, Oxford OX1 3QY, United Kingdom (richard.bailey@ouce.ox.ac.uk)

J. Faïn, Laboratoire de Physique Corpusculaire, 63177 Aubières Cedex, France (jean.fain@wanadoo.fr)

R. Grün, Research School of Earth Sciences, Australian National University, Canberra ACT 0200, Australia (rainer.grun@anu.edu.au)

T. Hashimoto, Department of Chemistry, Faculty of Sciences, Niigata University, Niigata 950-21, Japan (thashi@curie.sc.niigata-u.ac.jp)

D.J. Huntley, Department of Physics, Simon Fraser University, Burnaby B.C. V5A1S6, Canada (huntley@sfu.ca)

M. Lamothe, Dépt. Sci. de la Terre, Université du Québec à Montréal, CP 8888, H3C 3P8, Montréal, Québec, Canada (lamothe.michel@uqam.ca)

N. Mercier, Lab. Sci. du Climat et de l'Environ, CNRS-CEA, Av. de la Terrasse, 91198, Gif sur Yvette Cedex, France (norbert.mercier@lscce.cnrs-gif.fr)

D. Miallier, Laboratoire de Physique Corpusculaire, 63177 Aubières Cedex, France (miallier@clermont.in2p3.fr)

S.W.S. McKeever, Department of Physics, Oklahoma State University, Stillwater Oklahoma 74078, U.S.A. (stephen.mckeever@okstate.edu)

A.S. Murray, Nordic Laboratory for Luminescence Dating, Risø National Laboratory, Roskilde, DK-4000, Denmark (andrew.murray@risoe.dk)

N. Porat, Geological Survey of Israel, 30 Malkhe Israel St., Jerusalem 95501, Israel (naomi.porat@gsi.gov.il)

D. Richter, Lehrstuhl Geomorphologie, University of Bayreuth, 95440 Bayreuth, Germany (daniel.richter@uni-bayreuth.de)

D.C.W. Sanderson, Scottish Universities Environmental Research Centre, Scottish Enterprise Technology Park, East Kilbride G75 0QF, UK (David.Sanderson@glasgow.ac.uk)

A.K. Singhvi, Rm 203, Physical Research Laboratory, Navrangpura, Ahmedabad 380009, India (singhvi@prl.res.in)

K.J. Thomsen, Radiation Research Division, Risø National Laboratory for Sustainable Energy, Technical University of Denmark, DK-4000, Roskilde, Denmark (krth@risoe.dtu.dk)

Ancient TL

A periodical devoted to Luminescence and ESR dating

Web site: <http://www.aber.ac.uk/ancient-tl>

Department of Geography and Earth Sciences
Aberystwyth University SY23 3DB
United Kingdom

Tel: (44) 1970 622606

Fax: (44) 1970 622659

E-mail: ggd@aber.ac.uk

R package *numOSL*: numeric routines for optically stimulated luminescence dating

Jun Peng^{1,2*}, ZhiBao Dong¹, FengQing Han³, Hao Long⁴, XiangJun Liu³

¹Cold and Arid Regions Environmental and Engineering Research Institute, Chinese Academy of Sciences, 730000 Lanzhou, China

²University of Chinese Academy of Sciences, 100049 Beijing, China

³Qinghai Institute of Salt Lakes, Chinese Academy of Sciences, 810008 Xining, China

⁴Nanjing Institute of Geography and Limnology, Chinese Academy of Sciences, 210008 Nanjing, China

*Corresponding author: pengjun10@mails.ucas.ac.cn

(Received 27 August 2013; in final form 23 December 2013)

Abstract

In luminescence dating, there are various software packages that can be used to do data analysis, such as *Analyst*, *Java RadialPlotter*, *SigmaPlotTM* and so on. There is also an open source **R** package *Luminescence*, which has the capacity to tackle not only lots of basic statistical analysis but also provide more advanced data treatment. In this article, we present another **R** package, *numOSL*, the aim of which is neither to present a comprehensive numeric tool for luminescence dating just as the **R** package *Luminescence* did, nor to cover all numeric topics regarding luminescence dating. We focus only on the most frequently encountered numeric problems concerning luminescence dating, including equivalent dose calculation and error estimation, decay signal decomposition, fast-component equivalent dose calculation, and statistical age model optimization. Almost all our code is written in Fortran and is linked to **R** using an interface in order to improve algorithms, generality and flexibility. This makes it faster and perhaps more powerful when comparing to other numeric software.

Introduction

Basic numeric techniques are an important aspect of luminescence dating, which are frequently encountered in daily handling of luminescence data. These numeric techniques may include: 1) interpolation; 2) non-linear parameter optimization; 3) Monte-Carlo simulation; and 4) maximum likelihood estimation. Many software packages can be used to perform a special kind of numeric analysis for luminescence dating. For example, *Analyst* (Duller, 2007a) is mainly used for basic data handling such as data import/export, equivalent dose calculation, and plotting of graphs. *Java RadialPlotter* (Vermeesch, 2009) focuses on optimizing parameters in Galbraith's statistical age

models and drawing radial plots (Galbraith, 1988). *SigmaPlotTM* has been frequently employed to carry out decay curve fitting (Choi et al, 2006). However, if one wants to perform more flexible and more comprehensive analysis on a series of different kinds of data, such as curve fitting with decay signal data, or statistical age model analysis with equivalent dose (ED) values, no single software mentioned above can satisfy all the requests. There also is an open source **R** package *Luminescence* (Kreutzer et al, 2012, Dietze et al, 2013) written in pure **R** language, which contains more comprehensive numeric routines to analyze various kinds of luminescence data. Though flexible, sometimes pure **R** function run very slowly, which may impede its implementation in problems that need a great number of iterations or Monte-Carlo simulations.

R serves as excellent statistical software (Ihaka and Gentleman, 1996; R Core Team, 2013), and is free of charge. Most importantly, code written in **R** is available to the user and might be modified and redistributed. Another significant characteristic of **R** is that it can easily communicate with other programming languages such as *Fortran* and *C++*. Hence one can write the time-consuming part of a program in *Fortran* or *C++* and then link it to **R** using an interface to achieve acceptable running speed. This remains **R**'s flexibility and also makes it really powerful. In this paper, we introduce the **R** package *numOSL* as a toolbox for numeric optimizations that are frequently encountered in luminescence dating. To make it flexible and powerful, almost all our functions are written in *Fortran* and are linked to **R** using interface. The aims of this paper are: 1) unifying regular numeric routines in luminescence dating into handy functions and make them available to all users; 2) introducing the usage of these functions with examples.

Introduction to functions in R package *numOSL*

Function: *calED*

Currently, there are eight functions in package *numOSL* (Table 1). Function “*calED*” is used to fit a dose-response curve using the Levenberg-Marquardt algorithm and calculate an ED value by interpolation. Three models are provided (linear, exponential, linear plus exponential model) to do the fitting. For the linear model the fitting will not be a problem, but when it comes to an exponential or an exponential plus linear model, care needs to be taken regarding the choice of initial parameters. There are two options in function “*calED*” that can be used to initialize non-linear parameters: “*nstart*” and “*upb*”. “*upb*” is used to control the upper boundary of the *b* value in the non-linear model, which will be generated uniformly in the space (0, *upb*); then other initial values can be obtained with linear algebra method. For example, in an exponential model of the formula $y = a(1 - e^{-bx}) + c$, combining paired observations ($x_i, y_i, i=1, \dots, n$) with a uniformly distributed random *b* value, *a* and *c* can be calculated using a linear algebraic method. Then the Levenberg-Marquardt algorithm will be called to optimize those parameters. The process will be carried out repeatedly until stopping conditions are satisfied. The maximum allowed number of attempts is set to be “*nstart*”. The standard error of the ED value can be assessed using two methods (simple transform and Monte-Carlo simulation) outlined by Duller (2007b). Figure 1 is the outputted plot if we input the following commands to the **R** console:

```
library(numOSL)
Curvedata<-data.frame(cbind( c(0, 18, 36, 54, 72),
  c(0.03,1.49,2.51,3.32,4.0),
  c(0.002,0.05,0.12,0.34,0.37) ))
Ltx<-c(3.11, 0.131)
res<-calED(Curvedata, Ltx, model = "exp", nsim = 3000)
res
```

Function: *decomp*

Function “*decomp*” is a unified function for decay curve decomposition and can be applied either to CW-OSL or LM-OSL decay curves. Fitting decay curves is an ill-conditioned problem, and it is very sensitive to the choice of initial parameters. To make the procedure flexible and practicable, CW-OSL decay curves are fitted using a combination of a differential evolution method and the Levenberg-Marquardt algorithm as suggested by Bluszcz and Adamiec (2006). The general procedure for CW-OSL

Table 1: Available functions in version 1.0 of package *numOSL*

Function	Description
<i>calED</i>	Calculate an ED value and assess its standard error
<i>dbED</i>	Summarize the statistical characteristics of the distribution of ED values
<i>decomp</i>	Decompose CW-OSL or LM-OSL decay curves
<i>decompc</i>	Decompose CW-OSL or LM-OSL decay curves (plus a constant component)
<i>fastED</i>	Calculate a CW-OSL ED value using the fastest component
<i>print.RadialPlotter</i>	Print an object of class “ <i>RadialPlotter</i> ”
<i>RadialPlotter</i>	Optimize parameters of Galbraith’s statistical age models
<i>sgcED</i>	Calculate ED values using the standardized grow curve method

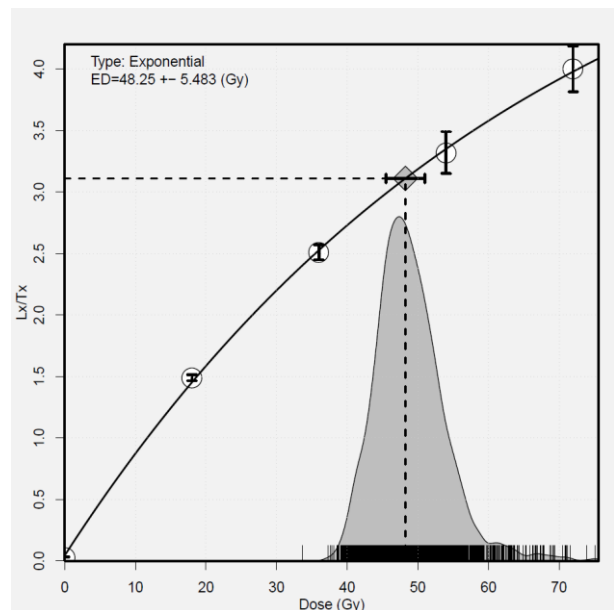


Figure 1: Plot output for function “*calED*”. The shaded area shows a gaussian kernel density plot for 3,000 ED values simulated with a Monte-Carlo technique.

fitting is: parameters are initialized using a differential evolution algorithm, and then using these initial parameters the Levenberg-Marquardt algorithm is employed for optimization. As pointed out by Bluszcz and Adamiec (2006), in some radical cases, the differential evolution algorithm (Storn and

Price, 1997) may fail, and we also note that sometimes parameters can be initialized with the differential evolution algorithm successfully but the Levenberg-Marquardt algorithm fails. If any of the two situations mentioned above occurs, a series of simple trials will be carried out, that is: detrapping rates are initialized to values outlined by Jain et al (2003) using permutation and combinations. For example, if we wish to decompose a given CW-OSL decay curve to 3 components, there will be $C(3,7)=35$ possible combinations of detrapping rates. Then for each possible combination of detrapping rates the number of trapped electrons that correspond to those detrapping rates can be obtained using a linear algebra method (Bluszcz, 1996) and these values will be used as initial parameters for the Levenberg-Marquardt algorithm. The above process is performed repeatedly until an acceptable result is found. Since the program is written in *Fortran* and wrapped with *R*, the whole procedure can be executed very quickly. The simple trial method described above is exactly the tactic we adopt in LM-OSL decay curves decomposing. Because we find it difficult to use the same method as used for fitting CW-OSL decay curves. The longer stimulation time makes it so time-consuming to conduct the differential evolution algorithm, even if all parts of the program are written in pure *Fortran*, that it becomes impracticable. Using the following commands in the *R* console we can obtain the plot shown in Figure 2 and Figure 3, respectively. The optional parameter “outfile” can be used to output decomposed signal values to a file and save it into the current work directory in “.csv” format (here the file will be “lmsig.csv”).

```
data(Signaldata)
print(decomp(Signaldata$sw[,1:2], ncomp=3, lwd=2))
res<-decomp(Signaldata$lm, ncomp=4, typ="lm",
            transf=TRUE, lwd=2, outfile="lmsig")
res
```

Function: fastED

A basic requirement for the application of the single-aliquot regenerative dose protocol (Murray and Wintle, 2000) is that the initial part of the OSL signal is dominated by the fast component (Li and Li, 2006). Generally, a fast-component ED value can be obtained through direct measurement (Bailey, 2010), component isolation with curve fitting (Cunningham and Wallinga, 2009) or integral channels selection (Cunningham and Wallinga, 2010). The function “fastED” attempts to build a fast-component growth curve to estimate a fast-component ED value using data obtained by the single-aliquot regenerative dose protocol (a series of decay curves). The number of

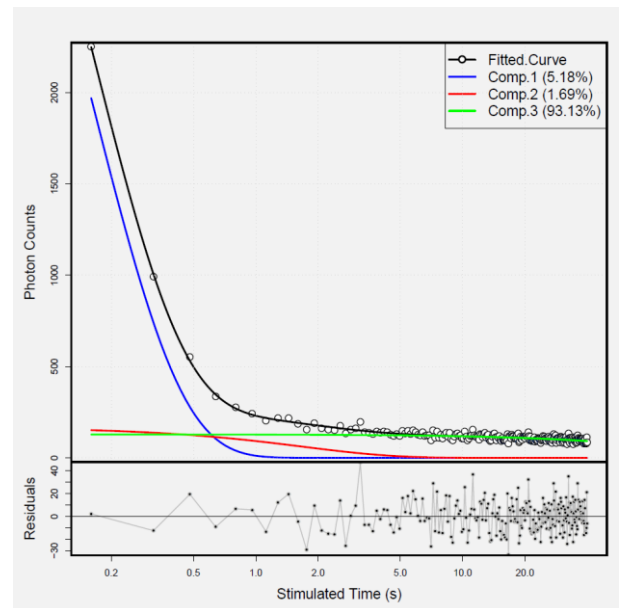


Figure 2: Decomposed 3 components for natural CW-OSL decay curve of sample GL1-1 (Peng and Han, 2013) using function “decomp”. The estimated parameters (magnitudes and decay rates) are given in table 3.

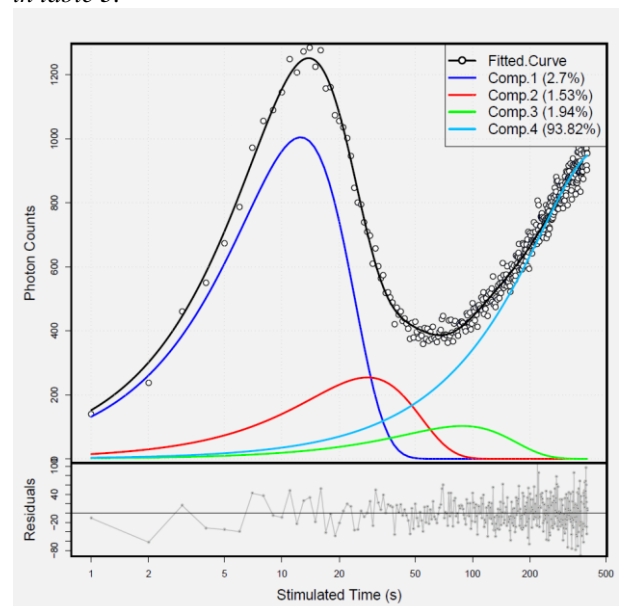


Figure 3: Decomposed 4 components for a LM-OSL decay curve (Li and Li, 2006) using function “decomp”. The estimated parameters are given in table 3.

trapped electrons that corresponds to the largest decay rate will be regarded as the fast-component signal, which cannot always ensure a pure fast-component signal to be extracted if ultra-fast component appears. The number of components to be decomposed is specified by the argument “ncomp”.

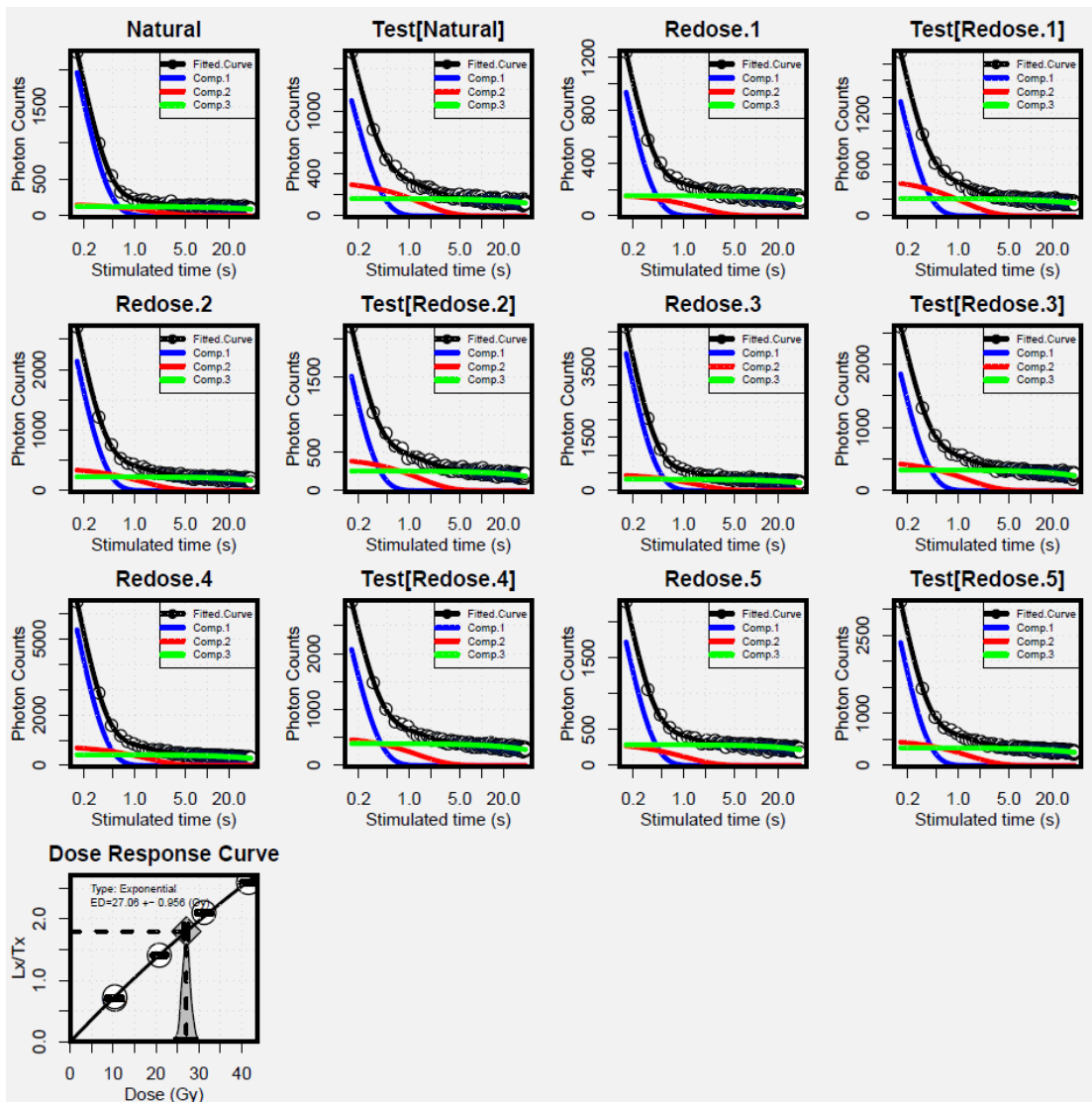


Figure 4: Result of fast-component ED estimation for sample GL1-1 with 3 components using function “fastED”. A total of 12 decay curves are decomposed and the growth curve is constructed with the extracted standardized fast-component signals.

During the calculation, the model used for growth curve fitting is chosen automatically with the principle of the minimum sum of square of residuals. Only CW-OSL data can be analyzed currently. We use sample GL1-1 (Peng and Han, 2013) as an example to show the usage of this function, the two decay curves that correspond to 0 regenerative dose are precluded before the analysis and each decay curve is decomposed to 3 components. The plot is shown in Figure 4:

```
fastED(Signaldata$sw[,c(-12,-13)],
ncomp=3, constant=FALSE,
Redose=c(80,160,240,320,80)*0.13)
```

The running time of the above process can be checked by **R** inner function “system.time” as:

```
system.time(fastED(Signaldata$sw[,c(-12,-13)],
ncomp=3, constant=FALSE,
Redose=c(80,160,240,320,80)*0.13))
```

Function: RadialPlotter

Function “RadialPlotter” is a unified function for optimizing a number of statistical age models as reviewed in Galbraith and Roberts (2012). It provides routines for the central age model (Galbraith et al, 1999), the finite mixture age model (Galbraith, 1988, Galbraith and Laslett, 1993) and the minimum age model (Galbraith et al, 1999). Depending on the specified model, it draws a radial plot automatically,

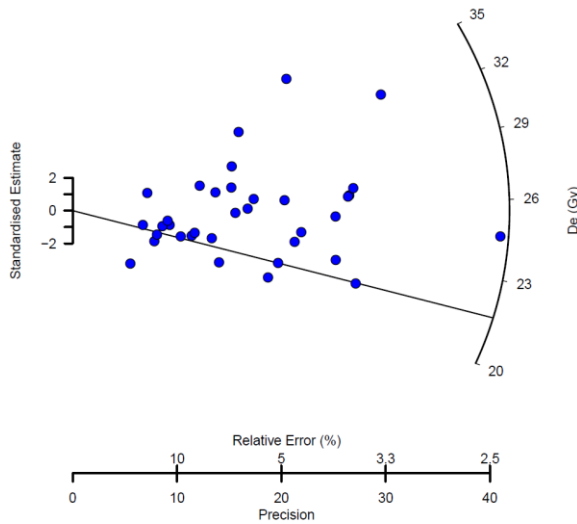


Figure 5: Radial plot output for 3-parameter minimum age model of sample GL1-1 with function “RadialPlotter”. The black line indicates estimated minimum ED value.

which works just like the *Java RadialPlotter* written by Vermeesch (2009). Both the central age model and the finite mixture age model are analyzed using the maximum likelihood estimation method outlined by Galbraith (1988). For minimum age models, it provides two numeric procedures to do the task: the “L-BFGS-B” algorithm (Zhu et al, 1994) and the “port” routine (the “port” algorithm is conducted using *R* inner function “nlminb” in package *stats*). The result returned by the function “RadialPlotter” is an object of class “RadialPlotter”. An example of using this function to fit a three-parameter minimum age model with sample GL1-1 is shown below, and the output is Figure 5:

```
data(EDdata)
obj<-RadialPlotter(EDdata$gl11,ncomp=-1,
  zscale=seq(20,37,3),kratio=0.6)
unclass(obj)
```

When attempting to fit the finite mixture model there is a parameter “maxcomp” that can be used to control the maximum allowed number of components. The function will search for the number of components that gives a minimum Bayesian Information Criterion (BIC) value (Schwarz, 1978) in the finite mixture model. Here we use sample AL3 (Schmidt et al, 2012) as an example to find out the most appropriate number of components. In the following codes, the maximum number of components is set to be 15. The radial plot created by this function is shown in Figure 6. A plot for BIC and maximized logged likelihood values against the number of components is shown in Figure 7, which

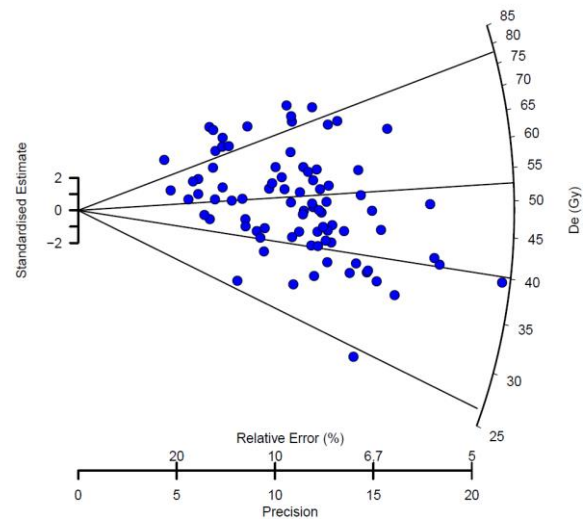


Figure 6: Radial plot output for finite mixture age model of sample AL3 with function “RadialPlotter”. The appropriate number of components that gives a minimum BIC value is found automatically at 4. The black lines are characteristic ED values for the estimated 4 components, respectively. The estimated parameters (proportion and characteristic ED value for each component) are summarized in table 4.

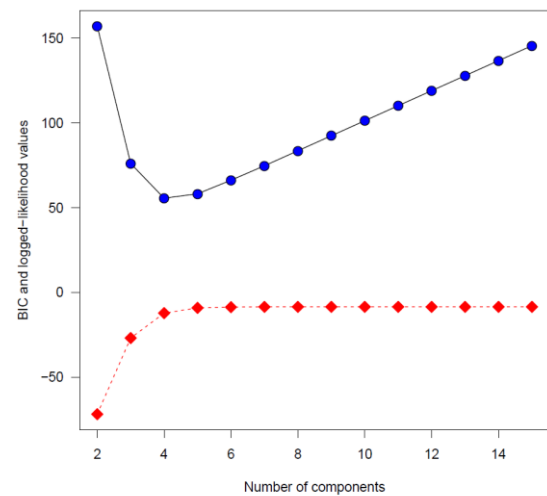


Figure 7: Variations of BIC and maximized logged-likelihood values with the number of components for sample AL3. The blue points are the BIC values while the red points are logged-likelihood values.

shows that 4 components given the minimum BIC value and should be regarded as the most appropriate number of components.

```
obj<-RadialPlotter(EDdata$al3, ncomp=0, maxcomp=15,
  zscale=seq(25,85,5), kratio=0.6)
print(obj)
```

Table 2: Comparing Duller's (2007b) results with that obtained using function "calED" in R package numOSL (version 1.0).

	R package numOSL			Duller (2007b)		
	ED	Curve fitting	Monte Carlo	ED	Curve fitting	Monte Carlo
Data 1	0.7	0.7±0.06	0.7±0.07	0.7	0.7±0.06	0.7±0.06
Data 2	28.5	28.5±0.67	28.5±0.76	28.5	28.5±0.67	28.5±0.75
Data 3	0.043	0.043±0.0056	0.043±0.002	0.046	0.046±0.004	0.046±0.001
Data 4	0.71	0.71±0.11	0.71±0.14	0.71	0.71±0.11	0.71±0.13

Table 3: Comparing results of decay curve decompositions obtained using function "decomp" in R package numOSL (version 1.0) with that obtained using SigmaPlot™ (version 10.0) and R package Luminescence (version 0.2.4) (Kreutzer et al, 2012) for natural CW-OSL decay curve of sample GL1-1 and LM-OSL decay curve of a quartz sample (Li and Li, 2006). a and b are estimated magnitude and decay rate for each signal component, respectively.

Component		R package numOSL		SigmaPlot™		R package Luminescence	
		a	b	a	b	a	b
CW-	#1	5240 ± 115	6.11 ± 0.16	5240 ± 104	6.11 ± 0.14	5240 ± 213	6.11 ± 0.30
OSL	#2	166.6 ± 25.8	0.59 ± 0.11	166.6 ± 21.0	0.59 ± 0.08	166.6 ± 6.28	0.59 ± 0.002
	#3	128.3 ± 3.40	0.008 ± 0.001	128.3 ± 2.94	0.008 ± 0.001	128.3 ± 48.0	0.008 ± 0.20
		residual = 43454		residual = 43453.65		residual = 43454	
LM-	#1	20769 ± 668	2.54 ± 0.065	20800 ± 663	2.54 ± 0.068	20771 ± 1759	2.54 ± 0.16
OSL	#2	11787 ± 520	0.51 ± 0.053	11798 ± 619	0.5 ± 0.048	11787 ± 3685	0.51 ± 0.13
	#3	14941 ± 1038	0.05 ± 0.007	14995 ± 1158	0.05 ± 0.006	14943 ± 4633	0.05 ± 0.018
	#4	721057 ± 25497	0.002 ± 0.0001	722659 ± 26461	0.002 ± 0.0001	721118 ± 65749	0.002 ± 0.0002
		residual = 373062.8		residual = 373066.02		residual = 373063	

Table 4: Comparing results of finite mixture age model obtained using Java RadialPlotter (version 4.4) (Vermeesch, 2009) and that obtained using function "RadialPlotter" in R package numOSL (version 1.0) for sample AL3 and sample GL1-1. The numbers of components (k) that give minimum BIC values are estimated automatically in the finite mixture age model. The spreads (sigma) in ED values are set to be 0.0.

	sigma=0.0	R package numOSL		Java RadialPlotter	
		k		k	
AL3		k=4		k=4	
		p ₁ =2.1%±1.8%	u ₁ =26.4±1.9	p ₁ =2.1%±1.8%	u ₁ =26.4±2.0
		p ₂ =35.1%±6.5%	u ₂ =40.1±0.7	p ₂ =35.2%±6.4%	u ₂ =40.1±0.7
		p ₃ =40.8%±6.7%	u ₃ =52.6±1.2	p ₃ =40.7%±6.7%	u ₃ =52.7±1.2
		p ₄ =22.0%±4.9%	u ₄ =77.9±2.2	p ₄ =22.0%±9.4%	u ₄ =77.9±2.2
GL1-1		k=3		k=3	
		p ₁ =37.6%±10.9%	u ₁ =22.0±0.4	p ₁ =38.0%±11.0%	u ₁ =22.0±0.5
		p ₂ =50.9%±11.3%	u ₂ =25.7±0.4	p ₂ =51.0%±11.0%	u ₂ =25.7±0.4
		p ₃ =11.5%±5.9%	u ₃ =33.7±0.9	p ₃ =11.0%±16.0%	u ₃ =33.8±0.9

Comparison with other software

The reliability of these routines was checked by comparing the results with those displayed in published articles or obtained using other software. The function "calED" was tested using the same data and results that were published in Duller (2007b) (Table 2); results obtained by function "decomp" are

compared to that obtained using SigmaPlot™ and R package Luminescence (Kreutzer et al, 2012) (Table 3); function "RadialPlotter" is checked by comparing the results with that estimated using Java RadialPlotter (Vermeesch, 2009) (Table 4). The results of all the tests are comparable between the different software packages.

Discussion and conclusion

Numeric techniques such as Monte-Carlo error simulation, and differential evolution are time-consuming tasks. Decomposing decay curves to various components and maximum likelihood estimations of Galbraith's statistical age models (especially the minimum age model) are ill-conditioned mathematical problems; whether it is possible to obtain a reasonable result depends heavily on the choice of initial parameters. Hence to make the program have the capacity to be applicable to a wide range of data sets, trying various initial parameters is indispensable, which, on the other hand, slows down the running speed. This problem will be especially significant if one wants to use the results to do some further analysis. For example, one may need to calculate ED values and assess their standard errors repeatedly when using the SGC method (Roberts and Duller, 2004). Alternatively if one hopes to decompose a series of decay curves to build a dose-response curve in order to calculate a fast-component ED value for data this requires general and fast routines.

In this paper, we present an **R** package (*numOSL*) for tackling regular numeric problems that are frequently encountered in analyzing luminescence data. This is the second **R** package concerning luminescence dating that is available on the Comprehensive **R** Archive Network (**CRAN**), but the work presented here is not a duplicated version for **R** package *Luminescence*. We focus only on regular numeric routines in luminescence dating and aim to make those routines more general and robust through a mixture programming language of **R** and *Fortran*. The tests show that results generated by package *numOSL* are comparable to other numeric packages. Flexible as it is, however, we must admit that users may need some basic knowledge about the **R** programming language when attempting to use an **R** package. So if one only needs to do some basic handling or plotting of luminescence data, the best choice would be *Analyst*, which is sufficient for rudimentary data processing and is user-friendly. The **R** package *numOSL* is provided under the General Public Licence (GPL3) conditions, which is free software and can be downloaded freely from <http://CRAN.R-project.org/package=numOSL>.

Anyone who finds a bug during the use of this package is encouraged to contact the corresponding author.

Acknowledgments

We thank Rex Galbraith and Sebastian Kreutzer for their permission to bundle their **R** code for radial plot drawing to **R** package *numOSL*. We also thank Andrzej Bluszcz, who offers lots of help during the writing of the differential evolution algorithm.

Sheng-Hua Li and Geoff Duller are thanked for helpful discussions concerning fast-component equivalent dose calculation. Silke Schmidt, Jeong-Heon Choi and Bo Li are thanked for providing published data to test our programs. This work was funded by the Ministry of Science and Technology of the People's Republic of China (2013CB956000 and 2012CB426501).

References

- Bailey, R.M. (2010). Direct measurement of the fast component of quartz optically stimulated luminescence and implications for the accuracy of optical dating. *Radiation Measurements* 5: 559-568.
- Bluszcz, A. (1996). Exponential function fitting to TL growth data and similar applications. *Geochronometria* 13: 135-141.
- Bluszcz, A., Adamiec, G. (2006). Application of differential evolution to fitting OSL decay curves. *Radiation Measurements* 41: 886-891.
- Choi, J.H., Duller G.A.T., Wintle, A.G. (2006). Analysis of quartz LM-OSL curves. *Ancient TL* 24: 9-20.
- Cunningham, A.C., Wallinga, J. (2009). Optically stimulated luminescence dating of young quartz using the fast component. *Radiation Measurements* 44: 423-428.
- Cunningham, A.C., Wallinga, J. (2010). Selection of integration time intervals for quartz OSL decay curves. *Quaternary Geochronology* 5: 657-666.
- Dietze M., Kreutzer, S., Fuchs, M.C., Burow, C., Fischer M., Schmidt, C. (2013). A practical guide to the R package Luminescence. *Ancient TL* 31: 11-18.
- Duller, G.A.T. (2007a). *Analyst*. Manual, p.1-45.
- Duller, G.A.T. (2007b). Assessing the error on equivalent dose estimates derived from single aliquot regenerative dose measurements. *Ancient TL* 25: 15-24.
- Galbraith, R.F. (1988). Graphical display of estimates having differing standard errors. *Technometrics* 30: 271-281.
- Galbraith, R.F., Laslett, G.M. (1993). Statistical models for mixed fission track ages. *Nuclear Tracks and Radiation Measurements* 21: 459-470.
- Galbraith, R.F., Roberts, R.G. (2012). Statistical aspects of equivalent dose and error calculation and display in OSL dating: An overview and some recommendations. *Quaternary Geochronology* 11: 1-27.
- Galbraith, R.F., Roberts, R.G., Laslett, G.M., Yoshida, H., Olley, J.M. (1999). Optical dating of single grains of quartz from Jinmium rock shelter, northern Australia. Part I: experimental design and statistical models. *Archaeometry* 41: 339-364.

- Ihaka, R., Gentleman, R. (1996). R: A Language for Data Analysis and Graphics. *J. Computational and Graphical Statistics* 5: 299-314.
- Jain, M., Murray, A.S., Boetter-Jensen, L. (2003). Characterisation of blue-light stimulated luminescence components in different quartz samples: implications for dose measurement. *Radiation Measurements* 37: 441-449.
- Kreutzer, S., Schmidt, C., Fuchs, M.C., Dietze, M., Fischer, M., Fuchs, M. (2012). Introducing an R package for luminescence dating analysis. *Ancient TL* 30: 1-8.
- Li, S.H., Li, B. (2006). Dose measurement using the fast component of LM-OSL signals from quartz. *Radiation Measurements* 41: 534-541.
- Murray, A.S., Wintle, A.G. (2000). Luminescence dating of quartz using improved single-aliquot regenerative-dose protocol. *Radiation Measurements* 32: 57-73.
- Peng, J., Han, F.Q. (2013). Selections of fast-component OSL signal using sediments from the south edge of Tengger Desert. *Acta Geoscientica Sinica* 34: 757-762 (In Chinese with English abstract).
- R Core Team. (2013). R: A language and environment for statistical computing. R Foundation for Statistical Computing, Vienna, Austria. URL <http://www.R-project.org/>.
- Roberts, H.M., Duller, G.A.T. (2004). Standardised growth curves for optical dating of sediment using multiple-grain aliquots. *Radiation Measurements* 38: 241-252.
- Schmidt, S., Tsukamoto, S., Salomon, E., Frechen, M., Hetzel, R. (2012). Optical dating of alluvial deposits at the orogenic front of the Andean precordillera (Mendoza, Argentina). *Geochronometria* 39: 62-75.
- Schwarz, G. (1978). Estimating the dimension of a model. *Annals of statistics* 6: 461-464.
- Storn, R., Price, K. (1997). Differential evolution: a simple and efficient adaptive scheme for global optimization over continuous spaces. *J. Global Optim.* 11: 341-359.
- Vermeesch, P. (2009). RadialPlotter: a Java application for fission track, luminescence and other radial plots. *Radiation Measurements* 44: 409-410.
- Zhu, C., Byrd, R.H., Lu, P., Nocedal, J. (1994). "L-BFGS-B: Fortran subroutines for large scale bound constrained optimization" Tech. Report, NAM-11, EECS Department, Northwestern University.

Reviewer

G.A.T. Duller

Optimising the reproducibility of measurements of the post-IR IRSL signal from single-grains of K-feldspar for dating

Smedley R.K. and Duller G.A.T.

Department of Geography and Earth Sciences, Aberystwyth University, Ceredigion, SY23 3DB, UK (e-mail: rks09@aber.ac.uk)

(Received 3 May 2013; in final form 13 December 2013)

Abstract

The reproducibility of the Risø single-grain measurement system has previously been quantified for the analysis of individual grains of quartz using the green laser and for single-grains of K-feldspar using the infrared (IR) laser at 50 °C. However, reproducibility estimates for a single-grain measurement system analysing K-feldspar grains using the post-IR IRSL (pIRIR) signal do not exist. This study provides the first measurement reproducibility estimates for both the pIRIR₂₂₅ and pIRIR₂₉₀ protocol using an IR laser. It is found that holding a sample at elevated temperatures (e.g. 225°C or 290°C) prior to measurement leads to loss of the pIRIR signal. The default single grain procedure implemented by the Risø reader may involve holding the sample at this elevated temperature for periods up to several hundreds of seconds, and that crucially this time may vary from one measurement to another, leading to poorer measurement reproducibility. The study demonstrates that the measurement procedure can be modified to standardise the time spent at high temperature (e.g. 290°C) and hence improve the reproducibility of the measurement system. The optimised procedure provides reproducibility estimates of 2.8 ± 0.3 % and 2.6 ± 0.3 % for the pIRIR₂₂₅ and pIRIR₂₉₀ signal, respectively, which are comparable to similar measurements performed with the green laser and the IR laser at 50 °C.

Introduction

Optically stimulated luminescence (OSL) dating with single-grains is a valuable approach in depositional environments where grains are likely to be incompletely-bleached. Single-grain dating involves analysing individual mineral grains (e.g. quartz or feldspar) to provide natural dose-distributions, which can then be statistically modelled to determine the true burial age. A major challenge for routine single-grain dating of sedimentary quartz from incompletely-bleached sediment is that typically only 5 % or fewer of the grains emit a detectable

OSL signal, e.g. as few as 0.5 % of quartz grains could be detected from glaciofluvial sediments from Chile (Duller, 2006). In contrast to quartz, a larger proportion of K-feldspar grains emit a detectable infrared stimulated luminescence (IRSL) signal (e.g. Duller et al. 2003). However, the IRSL signal of K-feldspars measured at ~50 °C (IR₅₀) is reported to ubiquitously suffer from anomalous fading, and therefore may require fading-correction to provide an accurate depositional age (Huntley and Lamothé, 2001). Thomsen et al. (2008, 2011) extensively studied the fading rates of feldspars in response to different stimulation and detection conditions, and suggested that a more stable post-IR IRSL (pIRIR) signal can be accessed within feldspar grains using an initial IRSL stimulation at 50 °C followed by an elevated temperature IRSL stimulation, typically performed at 225 °C or 290 °C, hereafter termed the pIRIR₂₂₅ and pIRIR₂₉₀ signals. Given that large and variable fading rates are often reported for single-grain K-feldspars measured using the IR₅₀ signal (e.g. Trauerstein et al. 2012), and also the difficulty in making accurate and precise fading measurements on individual grains, single-grain dating with K-feldspar would benefit from accessing the more stable pIRIR signal.

Measuring individual D_e values from single-grains normally results in more scatter in dose-distributions than is typical from multiple-grain analysis. Calculating the associated uncertainties in the D_e values for each grain requires knowledge of both the photon counting statistics and the reproducibility of the measurement system, though scatter may also arise from other factors that have not yet been identified. The reproducibility of the measurement system is dependent upon the thermal treatment, optical stimulation and material response for individual grains during measurement. Thus, measurement reproducibility is expected to vary between different readers used for single-grain measurements, the samples analysed, and between the IRSL and pIRIR signals used to measure K-feldspar grains. A challenge for IRSL analysis of K-

Step	IR ₆₀	pIRIR ₂₂₅	pIRIR ₂₉₀
1	Dose (100 Gy)	Dose (100 Gy)	Dose (100 Gy)
2	Preheat 250°C for 60 s	Preheat 250°C for 60 s	Preheat 320°C for 60 s
3	IR laser 2 s at 60°C	IR laser 2 s or LEDs 100 s at 60°C	IR laser 2 s or LEDs 100 s at 60°C
4	Test-dose (100 Gy)	IR laser 2 s at 225°C	IR laser 2 s at 290°C
5	Preheat 250°C for 60 s	Test-dose (100 Gy)	Test-dose (100 Gy)
6	IR laser 2 s at 60°C	Preheat 250°C for 60 s	Preheat 320°C for 60 s
7	IR laser 2 s or LEDs 100 s at 290°C	IR laser 2 s or LEDs 100 s at 60°C	IR laser 2 s or LEDs 100 s at 60°C
8		IR laser 2 s at 225°C	IR laser 2 s at 290°C
9		IR laser 2 s or LEDs 100 s at 290°C	IR laser 2 s or LEDs 100 s at 330°C

Table 1: Experimental details for the single-aliquot regenerative dose (SAR) pIRIR measurements performed throughout this study with the IR₆₀, pIRIR₂₂₅ and pIRIR₂₉₀ signals for single grains of K-feldspar. Note that the signal was measured for 0.15 s before and after the IR stimulation was performed so the IR laser was stimulating for a total duration of 1.7 s.

feldspars is the thermal-dependence of the magnitude of the signal (Duller and Wintle, 1991; McKeever et al. 1997), which has the potential to make measurement of the pIRIR signal less reproducible than that of IRSL signal. Calculating the reproducibility of the measurement system is important so that the appropriate uncertainty is incorporated into D_e estimates. However, measurement reproducibility estimates are not currently available for the Risø single-grain K-feldspar system using the pIRIR signal. Estimates of the reproducibility of the single-grain measurement system only currently exist for sedimentary grains of naturally-occurring quartz analysed using the green laser (e.g. Truscott et al. 2000; Thomsen et al. 2005; Jacobs et al. 2006) and K-feldspar analysis using the IR laser at 50 °C (e.g. Trauerstein et al. 2012).

Truscott et al. (2000) used an early prototype of the single-grain system equipped with a green laser to perform repeated L_x measurements on sensitised quartz grains to calculate a measurement reproducibility of 3.5 % per stimulation. Jacobs et al. (2006) subsequently repeated the measurements of Truscott et al. (2000) on sensitised grains of quartz to calculate the reproducibility of an improved single-grain laser system. The calculated mean measurement reproducibility estimate was 2.6 % (range ~1 – 8 %) and 1.3 % (range ~ 0.5 – 5 %) for optical stimulation times of 0.04 s and 0.3 s, respectively. The reproducibility improved when a longer summation interval was used as the decay rate is controlled by the power of the laser and this may vary slightly for individual stimulations; summing a larger part of the decay curve reduces the impact of the variable laser power during individual stimulations. Thomsen et al. (2005) also measured the reproducibility of a similar single-grain system with repeated L_x/T_x sensitivity-corrected measurements and calculated a mean (\pm standard error) of 2.5 ± 0.3 % and 1.5 % per OSL measurement for 0.03 s and 0.57 s of optical

stimulation, respectively, which is comparable to Jacobs et al. (2006). Finally, Trauerstein et al. (2012) adopted the approach of Thomsen et al. (2005) for single-grain analysis of K-feldspars using the IR₅₀ signal and calculated an estimate of reproducibility of 2.4 % (1 s of optical stimulation).

The principle aim of this study is to calculate the reproducibility of single-grain measurements of K-feldspar using the pIRIR signal. In addition, this study also aims to assess whether the reproducibility of the measurement system using the pIRIR signal can be optimised by (1) reducing the temperature at which the single-grain disc is held during disc location from the elevated temperature (i.e. 225 °C or 290 °C) to room temperature, and (2) using IR light emitting diodes (LEDs) instead of the IR laser to perform the low temperature measurements (here made at 60 °C) prior to the pIRIR measurements, and for bleaching grains at an elevated temperature at the end of each SAR cycle.

Experimental details

All luminescence measurements were performed using a Risø DA-15 automated TL/OSL single-grain system equipped with an IR laser (150 mW; 830 nm) (Bøtter-Jensen et al. 2003, Duller et al. 2003) at the Aberystwyth Luminescence Research Laboratory. The IR laser beam line was fitted with an RG-780 filter to remove any shorter wavelengths and a blue filter pack (Schott BG-39, GG-400 and Corning 7-59) was placed in front of the photomultiplier tube. The inclusion of the GG-400 filter is used to ensure complete removal of the thermally unstable UV transmission centred on 290 nm emitted during IR stimulation of feldspars (e.g. Balescu and Lamothe, 1992; Clarke and Rendell, 1997). The system was equipped with a $^{90}\text{Sr}/^{90}\text{Y}$ beta source delivering ~0.04 Gy/s. Table 1 outlines the protocols used for the three signals; IR₆₀, pIRIR₂₂₅ and pIRIR₂₉₀. Ten repeated

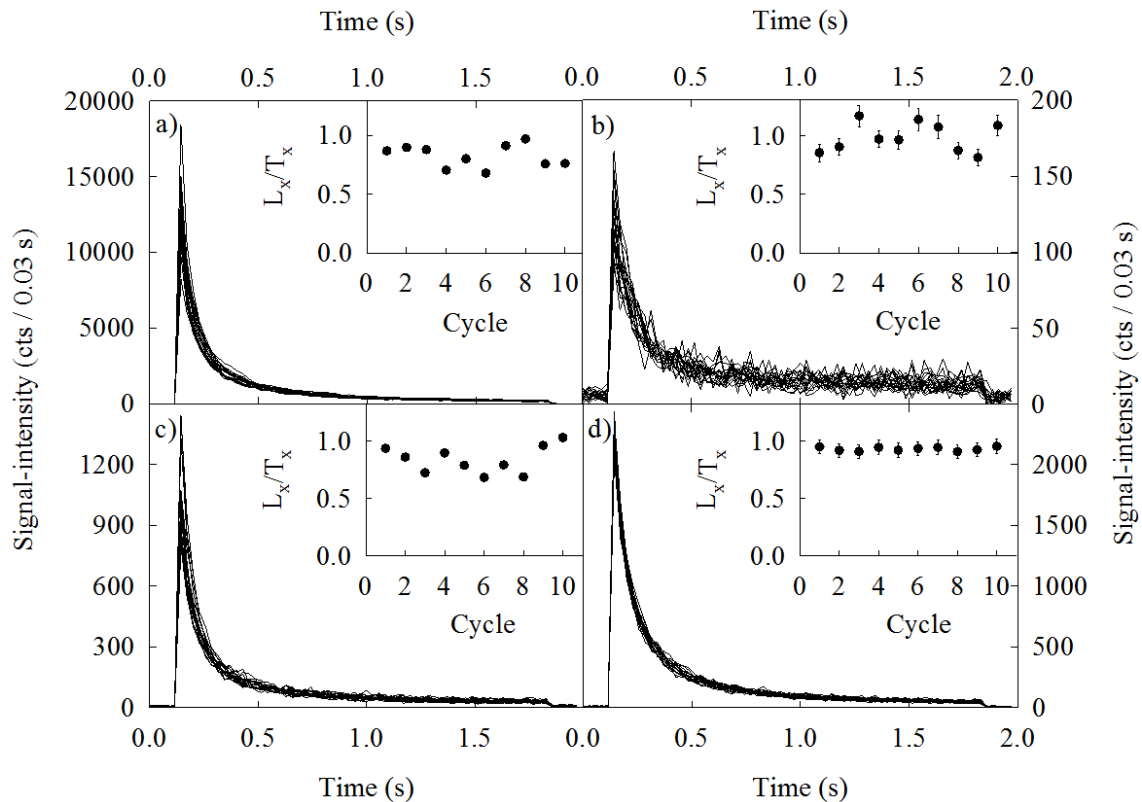


Figure 1: Examples of the repeated L_x and T_x decay curves measured with the $pIRIR_{225}$ signal for individual grains of K-feldspar from GDNZ13 for a) the brightest grain (measurement reproducibility of 12.0 %), b) the dimmest grain (measurement reproducibility of 8.9 %), c) the grain with the largest measurement error estimate (measurement reproducibility of 18.7 %) and d) the grain with the smallest measurement error estimate (measurement reproducibility of 0.6 %). The inserts show the change in L_x/T_x for the repeated measurements. Note that the disc location was performed at the elevated temperature of 225 °C and the IR bleaching throughout the protocol was performed with the IR laser.

L_x/T_x measurements were performed with the IR laser; 100 Gy doses were used to maintain an appropriate signal-intensity throughout analysis. The signal was recorded for a total of 2 s, which included the measurement of signal for 0.15 s before and after the IR stimulation was performed so the grains are stimulated using the IR laser for a duration of 1.7 s. The initial signal was summed over the first 0.3 s of stimulation and the background from the final 0.6 s. Grains were rejected if the test-dose uncertainty was greater than 10 %. The number of grains that fail this criterion varies for different measurement and analytical conditions, but this had no impact upon the patterns described in this study.

A sedimentary dune sand sample from New Zealand (GDNZ13) was used throughout this study. The sample was treated with a 10 % v.v. dilution of 37% HCl and 20 vols. of H_2O_2 to remove carbonates and organics, respectively. Dry sieving isolated the 180 – 212 μm diameter grains and density-separation provided the $< 2.58 \text{ g cm}^{-3}$ (K-feldspar) fraction. The K-feldspar grains were not etched in hydrofluoric

acid. The grains were mounted in aluminium single-grain discs (a 10 x 10 grid of 300 μm holes). All the experiments were repeated on exactly the same suite of K-feldspar grains, which remained in the single-grain disc throughout the analysis. Prior to these measurements the grains had been heated up to 330 °C and thus were not expected to exhibit large changes in sensitivity during this sequence of measurements.

The uncertainty arising from the reproducibility of the measurement system was calculated by subtracting in quadrature the uncertainty arising from the counting statistics from the observed uncertainty in the repeated L_x/T_x measurements following Section 7.1 of Thomsen et al. (2005). The uncertainty arising from the counting statistics for each individual grain was calculated using the equations outlined in Section 3 of Thomsen et al. (2005). The reproducibility of a single L_x measurement was then calculated from this value by dividing by $\sqrt{2}$ (Section 7.1, Thomsen et al. 2005). Fig. 1 presents examples of the L_x and T_x decay curves produced from

Protocol	IR ₆₀ bleach	High temperature bleach	Disc location temperature	Mean ± Standard error (%)	Standard deviation (%)	Range (%)	'n'
IR ₆₀	-	LEDs	60 °C	3.6 ± 0.3	2.4	0.3 – 10.0	49
pIRIR ₂₂₅	Laser	Laser	225 °C	5.9 ± 0.5	3.7	0.6 – 18.7	49
pIRIR ₂₂₅	Laser	Laser	60 °C	4.7 ± 0.4	3.1	0.5 – 14.6	48
pIRIR₂₂₅	LEDs	LEDs	60 °C	2.8 ± 0.4	2.8	0.3 – 10.9	45
pIRIR ₂₉₀	Laser	Laser	290 °C	4.7 ± 0.6	3.6	0.5 – 16.2	38
pIRIR ₂₉₀	Laser	Laser	60 °C	3.6 ± 0.4	2.4	1.0 – 11.3	43
pIRIR₂₉₀	LEDs	LEDs	60 °C	2.6 ± 0.3	1.8	0.2 – 8.2	36

Table 2: Measurement reproducibility estimates for the IR₆₀, pIRIR₂₂₅ and pIRIR₂₉₀ signals measured using the single grain system.

repeated single-grain pIRIR₂₂₅ measurements. For these measurements the disc location was performed at the elevated temperature of 225 °C prior to the stimulation at 225 °C. The default setting of the Risø system is for the disc location to be performed at whatever temperature the optical stimulation will occur. All of the data shown in Fig. 1 was collected using a sequence in which the IR laser was used for the measurements at 60 °C prior to the pIRIR measurement, and the IR laser was used for the elevated temperature bleaching at the end of each cycle (step 9 in Table 1). The examples shown in Fig. 1 include a) the brightest grain (12.0 % measurement reproducibility) and b) the dimmest grain (8.9 % measurement reproducibility) from the single-grain population, in addition to the grains with c) the largest (18.7 %) and d) the smallest (0.6 %) measurement reproducibility estimates calculated from the single-grain population.

Table 2 presents the mean and standard error measurement reproducibility estimates for the different protocols employed, including the range of estimates for individual grains. The range of IRSL reproducibility estimates in this study (0.3 – 10.0 %) covers a similar range to those obtained by Jacobs et al. (2006) for quartz using the green laser and 0.04 s of optical stimulation (~1 – 8 %). However, the mean IR₆₀ reproducibility estimate when the signal is summed over 0.3 s of optical stimulation (3.6 ± 0.3 %) is larger than the 2.4 % (1 s of optical stimulation) published by Trauerstein et al. (2012). When a longer summation interval is used (2 s of optical stimulation) then the IR₆₀ reproducibility becomes 2.6 ± 0.4 %, almost identical to that of Trauerstein et al. (2012) because the effects from the reproducibility of the laser have been removed. Initial estimates of the measurement reproducibility for pIRIR₂₂₅ and pIRIR₂₉₀ single-grain measurements prior to making any alterations to the protocol to optimise the

reproducibility were 5.9 ± 0.5 % and 4.7 ± 0.6 %, respectively (Table 2). Both estimates are larger than measurement reproducibility estimates presented here for the IRSL signal over comparable summation intervals (3.6 ± 0.3 %).

Optimising the reproducibility of the single-grain measurement system

Two aspects of the measurement procedure were modified in an attempt to optimise the reproducibility of the single-grain measurement system using the pIRIR₂₂₅ and pIRIR₂₉₀ signals; (1) reducing the temperature at which each disc is held during disc location prior to stimulation with the IR laser from the stimulation temperature (i.e. 225 °C or 290 °C) to room temperature, and (2) replacing the IR laser with the IR LEDs to perform the 60 °C measurements and the bleaches at an elevated temperature.

Reducing the temperature during disc location

The three locating holes present on each single-grain disc allow the Risø single-grain system to locate the exact position of the single-grain disc throughout the analysis (Duller et al. 1999). For single-grain measurements the software as installed by Risø is currently configured to heat the single-grain disc to the elevated temperature required for optical stimulation (i.e. 225 °C or 290 °C for the pIRIR protocols) prior to disc location, e.g. the single-grain disc is held at the elevated temperature whilst the system locates the exact position of the disc; a process which can take up to ~200 s and may vary throughout the sequence.

The reason why the disc is heated to whatever temperature is going to be used for optical stimulation before disc location occurs is that it was feared that heating of the disc may cause the disc to rotate (Thomsen, Pers. Comm.). If this occurred after disc location then the disc co-ordinates may be

a) Default tmsll.cmd script	b) Modified tmsll.cmd script
[SGOSL]	[SGOSL]
; \$1 Start Grain	; \$1 Start Grain
; \$2 Stop Grain	; \$2 Stop Grain
; \$3 Time	; \$3 Time
; \$4 Total Datapoints	; \$4 Total Datapoints
; \$5 Rate	; \$5 Rate
; \$6 PreHeat Temp	; \$6 PreHeat Temp
; \$7 Preheat Time	; \$7 Preheat Time
; \$8 Laser Power	; \$8 Laser Power
; \$9 Delay Before	; \$9 Delay Before
; \$10 Delay After	; \$10 Delay After
; \$11 Active Data points	; \$11 Active Data points
; \$12 LightSource	; \$12 LightSource
5=PS \$0	5=PS \$0
10=#RS	10=#RS
15=#WLT	15=#WLT
20=LU	20=LU
25=#RS	25=#RS
30=LV OFF	30=LV OFF
35=ST \$6 \$5	40=#FD \$12 \$0
40=#RS	50=#RS
42=PA \$7	55=LV ON
45=#RS	60=#RS
48=#FD \$12 \$0	62=ST \$6 \$5
50=#RS	64=#RS
55=LV ON	66=PA \$7
60=#RS	68=#RS
75=LA SET \$8	75=LA SET \$8
80=LI SET \$8	80=LI SET \$8
85=#LOOP \$1 \$2	85=#LOOP \$1 \$2
90=#INITGRAPH \$4	90=#INITGRAPH \$4
95=#SG #LOOPCOUNT \$12 \$3 \$4 \$11 \$10 \$9	95=#SG #LOOPCOUNT \$12 \$3 \$4 \$11 \$10 \$9
100=#DATA	100=#DATA
105=#RS	105=#RS
110=#ENDGRAPH	110=#ENDGRAPH
115=#SAVE	115=#SAVE
120=#ENDLOOP	120=#ENDLOOP
125=#APPEND	125=#APPEND
130=LD	127=ST 0
135=#RS	130=LD
	135=#RS

Table 3: The default (a) and modified (b) tmsll.cmd scripts from the latest version of TL/OSL sequence editor.

incorrect and this would affect the ability of the laser to accurately strike the grains during IRSL measurements.

In this study, the default command script (tmsll.cmd) originally installed with the software has been modified to undertake disc location at room temperature. Only once the position of the disc has been determined is the single-grain disc heated to the required temperature for the pIRIR measurement (i.e. 225 °C or 290 °C for the pIRIR protocols); this ensures that the period of time spent at elevated temperature is consistent from one set of single grain measurements to the next. The default tmsll.cmd script as installed by Risø and the modified

tmsll.cmd script of this study are presented in Table 3a and b, respectively. The key difference in the modified script is that the Find Disc (FD) command is now undertaken first (line 40) before raising the hotplate temperature (ST) to the desired measurement temperature (line 62).

Experiments were performed using the pIRIR₂₂₅ and pIRIR₂₉₀ signal on exactly the same suite of grains to assess the effect of reducing the disc location temperature from the elevated temperature (i.e. 225 °C or 290 °C) to room temperature. Table 2 presents the mean and standard error, and range in measurement reproducibility estimates for the different single-grain populations. The pIRIR₂₂₅

measurement reproducibility fell from 5.9 ± 0.5 % to 4.7 ± 0.4 % when the disc location was performed at 225 °C and room temperature, respectively, while the $pIRIR_{290}$ measurement reproducibility fell from 4.7 ± 0.6 % to 3.6 ± 0.4 %. Reducing the disc location temperature improved the mean measurement reproducibility by ~ 3 % for both signals (when subtracted in quadrature). Figure 2 presents the cumulative number of grains as a function of measurement reproducibility for the $pIRIR_{225}$ (circles) and $pIRIR_{290}$ (triangles) protocols using the disc location temperature of 225 °C or 290 °C (closed, solid line) and room temperature (open, dashed line). The corresponding single-grain populations are shown in the histograms for the $pIRIR_{225}$ (top) and $pIRIR_{290}$ (bottom) signals. The number of grains with measurement reproducibility estimates ≤ 2 % increases from 10 % to 16 % for the $pIRIR_{225}$ protocol and from 20 % to 30 % for the $pIRIR_{290}$ protocol when the disc location temperature is reduced to room temperature. The data shown here demonstrate that the reproducibility of the single-grain measurement system using the $pIRIR_{225}$ and $pIRIR_{290}$ signals of K-feldspar grains improves by reducing the disc location temperature to room temperature.

Why does the reproducibility improve when the disc location temperature is reduced?

The mean signal-intensity of all the single-grain K-feldspars on the single-grain disc was calculated for the sequences when disc location was performed at the elevated temperature and at room temperature. When the disc location temperature was reduced from the elevated temperature to room temperature the mean measured signal-intensity increased by ~ 23 % and ~ 34 % for the $pIRIR_{225}$ and $pIRIR_{290}$ signals, respectively. The lower mean signal-intensity measured when using an elevated disc location temperature suggests that the $pIRIR$ signal was thermally depleted throughout the period of time that it takes the single-grain measurement system to locate the disc. This thermal depletion would not occur if the disc was located at room temperature and could potentially explain the associated improvement in reproducibility. Additional experiments were performed to investigate whether thermal depletion of the $pIRIR$ signal during disc location at elevated temperatures can explain the improvement in the reproducibility of the single-grain K-feldspar measurements.

Experimental details

To assess whether loss of the $pIRIR$ signal could be observed due to holding the sample at elevated temperatures a multiple-grain aliquot of K-feldspar from sample GDNZ13 that had previously been

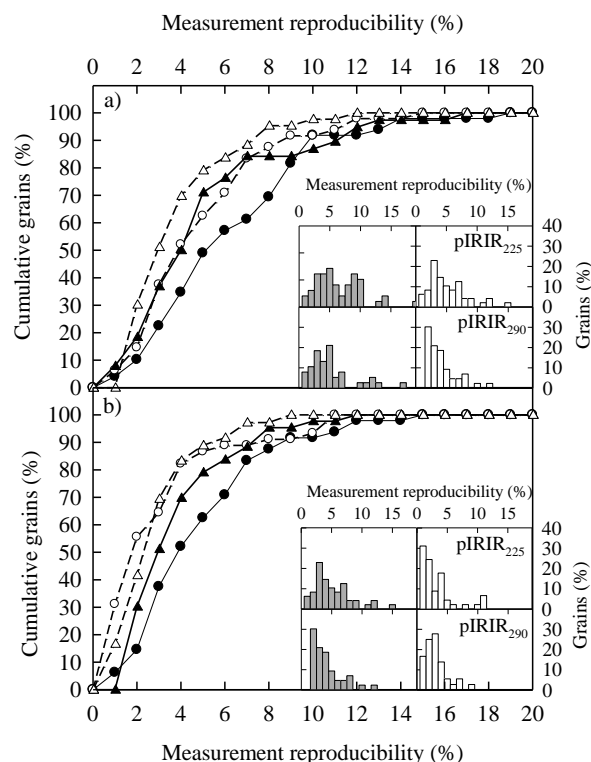


Figure 2: Measurement reproducibility as a function of cumulative grains for the experiments performed to optimise the reproducibility of the $pIRIR_{225}$ (circles) and $pIRIR_{290}$ (triangles) single-grain K-feldspar measurements. The histograms show the corresponding $pIRIR_{225}$ (top) and $pIRIR_{290}$ (bottom) single-grain populations. Data are shown (a) comparing measurements made with disc location at an elevated temperature (solid line; filled histogram) with those made at room temperature (dashed line, open histogram), and (b) comparing measurements made undertaking the IR bleach in the $pIRIR$ protocol with the focussed IR laser (solid line; filled histogram) to those undertaken with IR LEDs (dashed line; open histogram).

bleached using IR LEDs and heated up to 330 °C was subject to two experiments. Tables 4a and 4b describe the measurement sequences used for experiment 1 (pulsed stimulation using the IR LEDs) and experiment 2 (continuous stimulation using the IR LEDs), respectively. In both experiments any remnant charge was removed in step 1. The aliquot was then given a dose of 100 Gy (step 2) and preheated (step 3) using the same procedure (320 °C for 60 s) as that used normally for $pIRIR_{290}$ measurements, and used in Table 1. In experiment 2 the $pIRIR_{290}$ signal was measured continuously for 5 s, collecting data every 0.1 s, resulting in 50 data points. In experiment 1, 50 $pIRIR_{290}$ measurements were also performed, but they were carried out over a

Step	a) Pulsed IR LEDs	b) Continuous IR LEDs
1	IRSL at 330 °C for 100 s	IRSL at 330 °C for 100 s
2	100 Gy beta dose	100 Gy beta dose
3	TL 320 °C for 60 s	TL 320 °C for 60 s
4	IRSL at 60 °C for 100 s	IRSL at 60 °C for 100 s
5	Record TL signal as heating up to 290 °C	IRSL at 290 °C for 5 s
6	IRSL at 290 °C for 0.1 s every 10 s for 500 s	

Table 4: Experimental details for the multiple-grain *K*-feldspar experiments performed in this study.

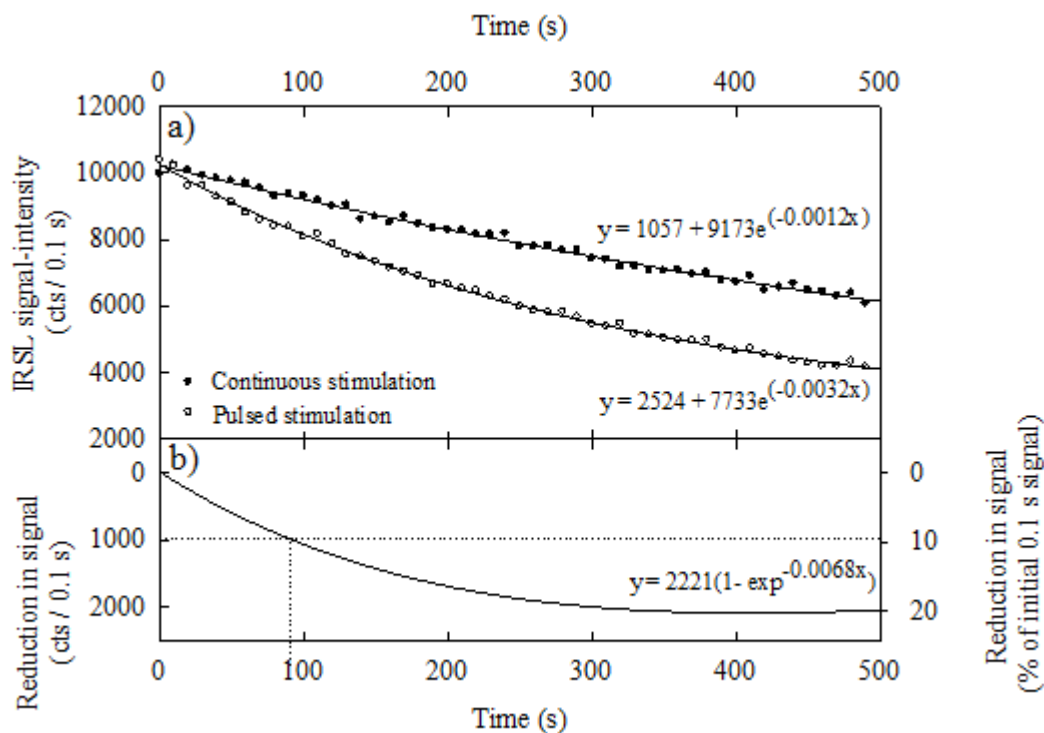


Figure 3: a) The pIRIR signal recorded during the pulsed 0.1 s IR LED measurements every 10 s for 500 s (Table 4, step 6a) and the continuous IR LED measurement (Table 4, step 5b). Both datasets have been fitted with an exponential function. b) The exponential fit from the pulsed IR LED measurements as presented in Fig. 3a is subtracted from the continuous IR LED measurement to determine the reduction in signal that can be attributed to the effects of the prolonged heating at 290 °C. The reduction in signal is presented in absolute counts (left y-axis) and as a percentage of the signal in the first 0.1 s of IR stimulation (right y-axis). The dashed line marks the calculated reduction in signal (1,016 cts / 0.1 s, 10 %) after holding the disc for 90 s at 290 °C as an example of what is typical during routine dating measurements.

period of 500 s. In both cases it is expected that the pIRIR signal will decrease due to optical eviction of charge, but if thermal depletion is also significant then the pulsed pIRIR data set collected over a longer period of time should show a greater decrease in intensity.

Reduction in signal-intensity when grains are held at an elevated temperature

The pIRIR₂₉₀ signals measured for the multiple-grain aliquot during the pulsed (experiment 1) and continuous (experiment 2) stimulation measurements

are shown in Fig. 3a; each dataset is fitted with an exponential function. The reduction in signal attributed to holding the multiple-grain aliquot at an elevated temperature was determined by subtracting the reduction in the pIRIR₂₉₀ signal measured during the continuous stimulation (experiment 2) from the reduction in the pIRIR₂₉₀ signal measured during the pulsed stimulation measurements (experiment 1). The subtracted data are presented in Fig. 3b as absolute counts (left y-axis) and as a percentage of the signal in the first 0.1 s of IR stimulation (right y-axis). Fig. 3b demonstrates that there is an exponential reduction

pIRIR measurement	Disc location time (min:sec)
L_n	03:44
T_n	01:12
L_x (0 Gy)	01:14
T_x (0 Gy)	02:06
L_x (24 Gy)	01:13
T_x (24 Gy)	01:13
L_x (48 Gy)	01:19
T_x (48 Gy)	01:11
L_x (96 Gy)	01:13
T_x (96 Gy)	01:14
L_x (0 Gy)	01:12
T_x (0 Gy)	01:13
L_x (24 Gy)	01:11
T_x (24 Gy)	01:12
Mean \pm st. dev.	01:12 \pm 00:36

Table 5: Periods of time it took the single-grain measurement system to locate the single-grain disc during a typical dating sequence using the pIRIR signal.

in signal caused by thermal depletion of the pIRIR signal at 290 °C where after 300 s (5 minutes) the signal has depleted by ~2000 cts / 0.1 s (~20 % of the initial 0.1 s of signal). Beyond 300 s the signal does not appear to deplete any further. The typical time taken for locating a single grain disc (~ 90 s) is marked on Fig. 3b. The calculated reduction in signal after holding the disc for 90 s at 290 °C was ~1000 cts / 0.1 s (~10 % of the initial 0.1 s of signal). Thus, these experiments show that the pIRIR signal-intensity measured for K-feldspar grains was thermally depleted when the grains were held at an elevated temperature.

Implications for single-grain dating of K-feldspars

The thermal depletion of the pIRIR signal when K-feldspar grains are held at elevated temperatures has important implications for single-grain analysis as the time it takes for the single-grain system to locate each disc prior to each L_x and T_x measurement is not constant throughout the measurement sequence. Table 5 presents an example of the different disc location times recorded throughout a typical dating sequence using the pIRIR signal. If the single-grain disc is held at an elevated temperature during the disc location, the pIRIR signals are thermally depleted for different periods of time throughout the sequence. Thus, the pIRIR signals measured are not comparable for each L_n , T_n , L_x and T_x measurement. Moreover, the single-grain measurement system typically finds it most difficult to locate the disc during the L_n

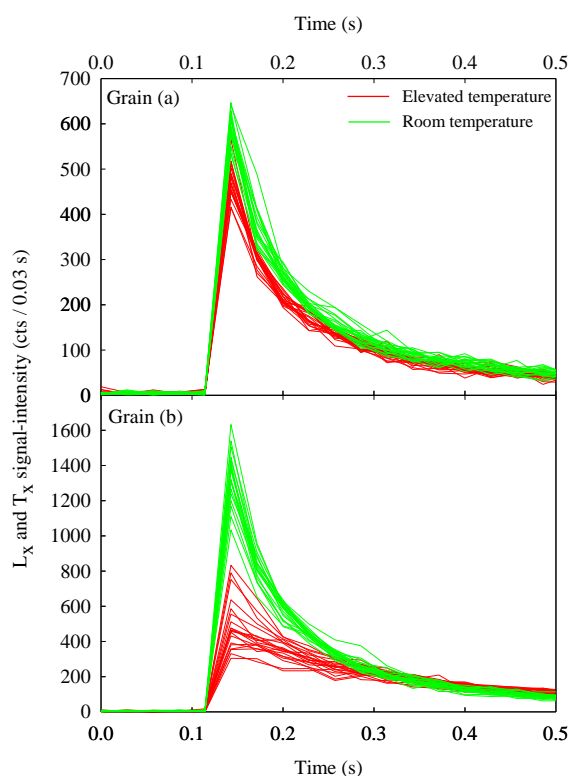


Figure 4: Examples of the initial 0.5 s of L_x and T_x decay curves measured during the reproducibility experiments performed with the disc location temperature at 290 °C and room temperature. Grain (a) gives the best reproducibility estimate, and is consistent between the experiments using disc location temperatures of 290 °C (1.0 %) and room temperature (1.3 %). In contrast, the reproducibility of grain (b) improves from 11.5 % to 1.7 % when changing the temperature of disc location from 290 °C to room temperature.

measurement (as shown in Table 5). Thus, it is likely that the L_n measurement is not comparable to the subsequent L_x and T_x measurements performed to construct the dose-response curve and provide sensitivity-correction.

Figure 4 shows two examples of the first 0.5 s of the L_x and T_x pIRIR₂₉₀ decay curves measured for two grains (denoted grains a and b) during the reproducibility experiments performed using disc location temperatures of 290 °C and room temperature. Grain (a) gave the lowest reproducibility estimate, and this did not improve when the disc location temperature was reduced to room temperature. Grain (b) gave a reproducibility estimate of 11.5 % when the disc location temperature was performed at 290 °C, but this fell to 1.7 % when disc location was performed at room temperature. The decay curves measured for grain (a) using disc location temperatures of 290 °C were generally

slightly lower intensity than the decay curves measured when the disc was repeatedly located at room temperature, but both sets of decay curves are very similar in shape. In comparison, the decay curves measured for grain (b) using disc location temperatures of 290 °C were more varied and dimmer than the decay curves measured when the disc was located at room temperature.

The decay curves shown for both grains (a) and (b) support the hypothesis that the pIRIR signals of the grains were thermally depleted for different durations of time for the L_x and T_x measurements when the disc location was performed at 290 °C. Comparing the different behaviours between grain (a) and (b) suggests that this effect was more pronounced in some grains in comparison to others; thus, the pIRIR signals of some of the K-feldspar grains were more thermally-dependent than other grains. Locating the discs at room temperature during single-grain dating can circumvent the issues associated with grain-to-grain variability in the thermal erosion of the pIRIR signal during disc location. Performing the disc location at room temperature should therefore be a preferred approach for all routine single-grain dating of sedimentary coarse-grained K-feldspar samples.

Replacing the IR laser with IR LEDs for bleaching

The pIRIR protocol typically incorporates two steps where IR stimulation is used to bleach the sample; one at 60 °C (step 3, Table 1) to remove the influence of any unstable IR_{60} signal prior to the elevated temperature stimulation (i.e. 225 °C or 290 °C), and a second at an elevated temperature (i.e. 290 °C or 330 °C, step 9, Table 1) to prevent charge transfer between SAR cycles. The experiments performed using the pIRIR protocol in this study compared the difference between using the focussed IR laser and the IR LEDs for these two bleaching steps. Table 2 presents the mean, standard error, and range in measurement reproducibility estimates for the individual grains analysed. The mean measurement reproducibility reduced from 4.7 ± 0.4 % to 2.8 ± 0.4 % for the pIRIR₂₂₅ signal, and from 3.6 ± 0.4 % to 2.6 ± 0.3 % for the pIRIR₂₉₀ signal when using the IR LEDs to bleach the grains instead of the IR laser. The measurement reproducibility measured after modifying the pIRIR₂₂₅ and pIRIR₂₉₀ protocols are now comparable with that of the IRSL signal in this study and those published for the green laser (2.5 ± 0.3 %, Thomsen et al. 2005) and the IR laser at 50 °C (2.4 %, Trauerstein et al. 2012).

Figure 2b presents the grains as a function of measurement reproducibility estimates calculated for the pIRIR₂₂₅ (circles) and pIRIR₂₉₀ (triangles) signals using the IR laser (closed, solid line) and IR LEDs (open, dashed line) for bleaching during the measurement protocol. Histograms of the single-

grain populations for the pIRIR₂₂₅ (top) and pIRIR₂₉₀ (bottom) signals plot the percentage of grains as a function of the measurement reproducibility and are also shown as inserts in Fig. 2b. Fig. 2b demonstrates the large improvement in the individual estimates of measurement reproducibility for the single-grain population when the IR LEDs are used for bleaching in the pIRIR protocol instead of the IR laser. The range in individual grain measurement reproducibility for the pIRIR₂₂₅ (0.3 – 10.9 %) and pIRIR₂₉₀ (0.2 – 8.2 %) is now comparable to the IR_{60} measurements in this study (0.3 – 10.0 %).

Conclusion

The Risø single-grain measurement system can be optimised to improve the reproducibility of the single-grain measurement system using the pIRIR signal of K-feldspars, and now provides estimates comparable to published single-grain quartz (Jacobs et al. 2006; Thomsen et al. 2005) and IR_{50} K-feldspar measurements (Trauerstein et al. 2012). Reducing the disc location temperature during pIRIR measurements from an elevated temperature (225 °C or 290 °C) to room temperature improves the measurement reproducibility by an average of ~3 % for the single-grain population. In addition, the use of IR LEDs instead of the IR laser to perform the bleaching at 60 °C and at elevated temperatures at the end of each SAR cycle improved the measurement reproducibility further to the estimates of 2.8 ± 0.3 % and 2.6 ± 0.3 % for the pIRIR₂₂₅ and pIRIR₂₉₀ signal, respectively. Both adaptations to the measurement of single-grain K-feldspars using the pIRIR signal are demonstrated to optimise the reproducibility of the single-grain measurement system; thus, the authors recommend that similar experiments are performed for individual readers to quantify the reproducibility of the equipment and measurement protocol used for single-grain dating.

Acknowledgements

Financial support was provided by a NERC PhD studentship to RKS (NE/1527845/1). Dr Kristina Thomsen is thanked for confirming the calculations of measurement reproducibility in this study and her valuable comments that helped to improve the quality of this manuscript.

References

- Balescu, S. and Lamothe, M. (1992). The blue emission of K-feldspar coarse grains and its potential for overcoming TL age underestimation. *Quaternary Science Reviews* 11: 45 – 51.

- Bøtter-Jensen, L., Andersen, C.E., Duller, G.A.T., and Murray, A.S. (2003). Developments in radiation, stimulation and observation facilities in luminescence measurements. *Radiation Measurements* 37: 535-541.
- Clarke, M.L. and Rendell, H.M. (1997). Infra-red stimulated luminescence spectra of alkali feldspars. *Radiation Measurements* 27: 221 – 236.
- Duller, G. A. T. (2006). Single grain optical dating of glacial deposits. *Quaternary Geochronology* 1: 296 – 304.
- Duller, G.A.T. and Wintle, A.G. (1991). On infrared stimulated luminescence at elevated temperatures. *Nuclear Tracks and Radiation Measurements* 18: 379 – 384.
- Duller, G.A.T., Bøtter-Jensen, L., Kohsiek, P. and Murray, A.S. (1999). A high-sensitivity optically stimulated luminescence scanning system for measurement of single sand-sized grains. *Radiation Protection Dosimetry* 84: 325-330.
- Duller, G.A.T., Bøtter-Jensen, L., and Murray, A.S. (2003). Combining infrared- and green-laser stimulation sources in single-grain luminescence measurements of feldspar and quartz. *Radiation Measurements* 37: 543 – 550.
- Huntley, D.J. and Lamothe, M. (2001). Ubiquity of anomalous fading in K-feldspars and the measurement and correction for it in optical dating. *Canadian Journal of Earth Sciences* 38: 1093 – 1106.
- Jacobs, Z., Duller G.A.T. and Wintle, A.G. (2006). Interpretation of single-grain D_e distributions and calculation of D_e . *Radiation Measurements* 41: 264 – 277.
- McKeever, S.W.S., Bøtter-Jensen, L. Agersnap, N. and Duller, G.A.T. (1997). Temperature dependence of OSL decay curves: experimental and theoretical aspects. *Radiation Measurements* 27: 161 – 170.
- Thomsen, K.J., Murray, A.S., and Botter-Jensen, L (2005). Sources of variability in OSL dose measurements using single grains of quartz. *Radiation Measurements* 39: 47 – 61.
- Thomsen, K.J., Murray, A.S. and Jain, M. (2011). Stability of IRSL signals from sedimentary K-feldspar samples. *Geochronometria* 38: 1 – 13.
- Thomsen, K.J., Murray, A.S., Jain, M. and Bøtter-Jensen, L. (2008). Laboratory fading rates of various luminescence signals from feldspar-rich sediment extracts. *Radiation measurements* 43: 1474 – 1486.
- Trauerstein, M., Lowick, S., Pressuer, F., Rufer, D. and Schlunegger, F. (2012). Exploring fading in single-grain feldspar IRSL measurements. *Quaternary Geochronology* 10: 327 – 333.
- Truscott, A.J., Duller, G.A.T., Botter-Jensen, L., Murray, A.S., and Wintle, A.G. (2000). Reproducibility of optically stimulated luminescence measurements from single grains of $Al_2O_3:C$ and annealed quartz. *Radiation Measurements* 32: 447 – 451.

Reviewer

K. J. Thomsen

Thesis Abstracts

Author: Gong Zhijun
Thesis Title: Application of optical dating to late Quaternary uplift and thrust activity in the northern piedmont of the Tian Shan, China
Grade: Ph.D.
Date: August 2012
Supervisors: Sheng-Hua Li
Address: Department of Earth Sciences, The University of Hong Kong, Hong Kong

Tian Shan is one of the most important orogenic belts in central Asia. It has been reactivated as a result of the Cenozoic India-Eurasia collision. Dating of the late Cenozoic tectonic deformation of Tian Shan and its piedmonts is important for understanding the mountain building as well as evaluating seismic hazards in the region. This study is focused on the applications of optical dating to the late Quaternary uplift and thrust activity along Manas River, in the northern piedmont of the Tian Shan, China.

The sediments on river terraces were dated with optical dating. The elevations were measured with the kinematic global position system (GPS). The results suggest that two phases can be identified according to the significantly different river incision rates. One phase was from ~20 ka to ~4.8 ka, with a much slower incision rate of $\sim 2.2 \pm 0.6$ mm/yr. The other phase was from ~4.8 ka to present, with a faster incision rate of $\sim 13.5 \pm 0.6$ mm/yr. The accelerated incision rate of Manas River was mainly attributed to the tectonic forces, suggesting that the tectonic uplift was significantly intensified since ~4.8 ka in the northern piedmont of Tian Shan.

The study region has suffered from multiple thrust activities during the late Quaternary, which led to the intensively deformations of the river terraces. By studying the deformed terraces, I evaluated the timing of the past thrust activities as well as the vertical slip rate of the thrust faults. The results demonstrated that the thrust activity intensified during the late Holocene, as manifested by the more frequent thrust activities and higher vertical slip rates.

Both quartz and potassium feldspar can be as dosimeters for optical dating of sediments. However, quartz OSL is sometimes seriously impeded with problems such as very dim signals and insufficient bleaching problems. K-feldspar has attractive advantages over quartz, despite of problem of anomalous fading. K-feldspar was explored in this

study, by investigating the relationship between the infrared stimulated luminescence (IRSL) and blue light stimulated luminescence (BLSL) signals. For IRSL and BLSL at 60 °C, it was suggested that most of the IRSL could be bleached by blue light (BL), while the BLSL could only be partially bleached by infrared (IR) stimulation. Besides, the fast and medium components of BLSL were mainly associated with the IRSL. If IR stimulation temperature was raised from 60 to 200 °C, at least two portions of the IRSL signals at 200 °C were observed. One portion could be bleached by BL at 60 °C and the other portion was hardly bleached by BL at 60 °C. Dating of K-feldspar from the various signals provided cross-checking for the reliability of quartz OSL for dating sedimentary samples.

Author: Julie A. Durcan
Thesis Title: Luminescence dating of sediments in Punjab, Pakistan: implications for the collapse of the Harappan Civilisation
Grade: Ph.D.
Date: December 2012
Supervisors: Geoff A.T. Duller, Mark G. Macklin
Address: Institute of Geography and Earth Sciences, Aberystwyth University, UK

This study presents the first application of optically stimulated luminescence (OSL) dating in the lowlands of Pakistan. More specifically, the Pakistani section of the Ghaggar-Hakra palaeochannel is dated for the first time, having been the subject of research for over a century. The Ghaggar-Hakra is associated with a dense concentration of Mature and Late Harappan archaeological sites. The Mature Harappan are hypothesised to have collapsed at ~3.9 ka, and it has been hypothesised that changing fluvial activity and climatic variability were key factors in the demise of this civilisation. This thesis aims to use OSL dating to develop a chronology of fluvial activity for the palaeochannel and to establish whether there is a temporal link between changing fluvial activity and climatic variability. The chronology is also compared with records of archaeological change to ascertain whether changing

fluvial activity contributed to the Mature Harappan collapse.

The majority of work presented in this thesis is concerned with the development of an accurate geochronological framework using OSL dating. The fast ratio is developed as a means for assessing the dominance of the fast component in the initial part of a quartz OSL signal and range-finder OSL dating is developed as a protocol for rapid age estimation using the quartz OSL signal, providing age estimates with uncertainties within 20%. Equivalent dose calculation using statistical models is discussed and the extent of incomplete bleaching in the dataset is considered. OSL ages dating predominantly from the Holocene are presented.

Based on the OSL ages calculated, strengthened fluvial activity in the Ghaggar-Hakra palaeochannel during the early and mid-Holocene is observed. Flow recession up-channel during the mid-Holocene is inferred, and a hiatus in fluvial deposition in the channel is observed between 4.5 and 1.4 ka. Changes in fluvial activity in the Ghaggar-Hakra are driven by the intensity of the Asian Monsoon, which fluctuates during the Holocene. Changing fluvial activity coincides with documented archaeological change and it is concluded that changing fluvial activity driven by climate was a significant factor in the collapse of the Mature Harappan at ~3.9 ka.

Author: Alicia Medialdea
Thesis Title: Towards the reconstruction of flood histories: Luminescence dating of palaeoflood deposits
Grade: Ph.D.
Date: February 2013
Supervisors: Gerardo Benito and Kristina Thomsen
Address: Museo Nacional de Ciencias Naturales-CSIC, Madrid, Spain / Universidad Autonoma de Madrid, Spain / Centre for Nuclear Technologies, Risø DTU, Denmark

The accurate dating of palaeoflood deposits plays a key role in the understanding of river flooding events, which are one of the main natural hazards related to climate, causing severe damage on mankind's life. The latest developments in the measuring and data analyses applied to optically stimulated luminescence dating (OSL) have made this technique highly reliable to assess chronologies for Quaternary

processes. But in some cases OSL can be hampered and the achievement of accurate ages becomes a challenge. This is the case of young flash-flood deposits which are likely to be affected by incomplete bleaching and in which any extrinsic factor could lead to a dramatic misestimate of the burial age.

Flood sediments from four rivers of the Iberian Peninsula (Guadalentín, Rambla de la Viuda, Huebra and Duero) have been sampled, covering a wide variety of environments for this thesis. A sequence of eight modern (40-1000 years) flash-flood deposits, potentially affected by incomplete bleaching, with available age control from historical records and radiocarbon ages has been used as reference values. Results from measurement of small (~30 grains) multi-grain aliquots have been compared to those derived from single grains. Burial ages have been estimated by using descriptive and robust statistics, the Central Age Model (CAM), Minimum Age Model (MAM) and Internal-External Consistency Criteria (IEU). A data transformation has been proposed in order to apply CAM and MAM models to dose distributions containing zero and negative values. All approaches have been applied to both, multi-grain and single grain doses.

The effect of the assumed over-dispersion on the burial dose estimation has been studied in detail finding a moderate effect when applying IEU approach and a very strong effect when using MAM model. Over-dispersion has been assigned based on dose recovery experiments measured on bleached/gamma dosed samples.

Comparison of the different OSL burial dose estimates with the independent age control indicates that best ages are achieved when using IEU approach. Consistent results are found for small multi-grain aliquots and single grains, showing that small (~30 grains) multi-grain aliquots in combination with minimum age models (i.e. IEU, MAM) are suitable for age estimation even in samples with high percentage (up to of incompletely bleached grains). Achieved conclusions have been applied to date the samples from the remaining three rivers. In all cases the estimated ages are consistent with the stratigraphy.

Author: Yiwei Chen
Thesis Title: Optical dating investigation into the slip rate of Altyn Tagh Fault and evolution of Zhari Namco, Tibetan Plateau
Grade: Ph.D.
Date: March 2013
Supervisors: Sheng-Hua Li
Address: Department of Earth Sciences, The University of Hong Kong, Hong Kong

New applications of the optically stimulated luminescence (OSL) dating were carried out with the aim of understanding late Quaternary activities for the Tibetan Plateau. This included studying the slip rate of the Altyn Tagh Fault, northeast Tibetan Plateau, and revealing the environmental changes derived from large inland lake's evolution, central south Tibet.

Two deflected streams across the Altyn Tagh Fault close to Aksay (39°24.572'N, 94°16.012'E) were investigated. Geomorphological analysis suggests that loess covering deflected stream banks has recorded past faulting events. A conceptual model is proposed illustrating the relationship. OSL dating of sixteen loess samples at both streams support the model, suggesting the loess is deposited episodically after fault strikes and subsequent channel wall refreshment. The age and offset indicate a slip rate of 11 ± 2 mm/yr for this part of the Altyn Tagh Fault.

Another river section near Aksay was also investigated for the slip rate information. Two risers between three terraces are clearly offset; OSL dating of loess covering terrace surfaces yielded terrace ages. Using the upper-terrace age to represent riser displacement duration, the rate is estimated to be 12 ± 1 mm/yr. The result suggests that using upper terrace is more suitable in this region. Notably, though, the slow rate is at odds with proposals that assume high-speed extrusion (~23 mm/year) of the Tibetan Plateau being accommodated by the Altyn Tagh Fault.

Palaeo-shorelines around the third largest lake in Tibet, Zhari Namco, were for the first time systematically investigated using OSL dating. Twenty-two sediment samples from eleven shorelines indicate that the water level has dropped ~128 m and the lake has undergone stepwise shrinkage since 8.2 ka. Digital elevation model calculation indicates the lake has shrunk from 4605 km² in size at 8.2 ka to 996 km² at present, which is equivalent to ~300 km³ of water. This implies a significant reduction in precipitation over the past 8.2 ka, a result of weakening Indian Monsoon or a shift of monsoon circulation path. The result is consistent with other

lake-core, ice-core climate proxies and solar insolation changes, implying the dominance of a weakening Indian Monsoon over central Tibet in the Holocene. Using the elevation of the highest shoreline of the four largest lakes in Tibet, the early Holocene Pan-lake hypothesis is proposed for the central Tibet.

In addition to these applications of OSL dating, technical studies on sensitivity changes and residual doses have been carried out for potassium rich feldspar (K-feldspar). Recent development of infrared stimulated luminescence (IRSL) signals from K-feldspar has shown great potential for extending the datable range for OSL dating. Sensitivity changes and residual doses of post-IR IRSL and multi-elevated - temperature post-IR IRSL protocols for K-feldspar were studied. A sensitivity decrease is observed after adopting a high temperature IRSL. IRSL signals stimulated at high temperature are found to contain large residual doses. The residual dose rises with stimulation time, suggesting that the initial part of IRSL signals contains more easy-to-bleach signals comparing with the later part.

Author: Carly Leighton
Thesis Title: Desert dune system response to Late Quaternary environmental change in the northeastern Rub' al Khali: Advances in the application of optically stimulated luminescence datasets
Grade: Ph.D.
Date: November 2013
Supervisors: Richard M. Bailey, David S.G. Thomas
Address: School of Geography and the Environment, OUCE, University of Oxford, South Parks Road, Oxford. OX1 3QY

The application of optically stimulated luminescence (OSL) dating to desert sand dunes has allowed accumulation histories to be used as tools to infer past environmental change. In response to issues facing the interpretation of these records, two research questions are addressed in this thesis. (i) Are dune chronologies representative of dune stratigraphies? And (ii) how can we most appropriately interpret dune chronologies as records of Quaternary environmental conditions?

Five dune profiles were sampled for OSL dating at two sites in the northeastern Rub' al Khali in the southern Arabian Peninsula. The visible stratigraphy

was used to guide sampling for three of the profiles and the effectiveness of this approach is assessed. A key finding is that bounding surfaces are not always identifiable as chronological hiatuses by OSL dating, given the level of precision that can be achieved. Using hierarchical relationships visible in two-dimensional exposures is therefore not guaranteed to identify the depositional units necessary to reconstruct dune histories.

Comparison of the depositional records from three sampled profiles shows that there is significant variability in chronologies at both the dune and dunefield scales. In light of these findings, the use of 'range-finder' OSL dating was investigated as a method of increasing sample throughput in the laboratory. It is concluded that the use of partially prepared samples and shortened measurement techniques can be used to rapidly assess the chronological context of samples and target those units most useful in constructing dune profiles.

A new method of presenting dunefield OSL datasets as net accumulation rates, incorporating accumulation thickness rather than relying on the frequency of ages, is presented. Within the last 30 ka, regional accumulation and preservation occurred at ~30-26, 22.5-18, 16-9, 6-2.7, 2.1-1.6, 1.1 and 0.7 ka. In conjunction with numerical model results and a review of other palaeoenvironmental archives, the regional aeolian record is interpreted as a response to changing forcing factors. High rates of net accumulation between ~16-9 ka are attributed to coeval increases in sediment supply and transport capacity. A hiatus in accumulation between ~9-6 ka is interpreted as a result of reduced sediment availability due to high moisture levels. The importance of both external forcing factors and local controls on dune accumulation processes is recognised, and therefore the importance of sampling at multiple locations to distinguish these factors is emphasised.

Bibliography

Compiled by Daniel Richter

From 1st April 2013 to 30th November 2013

- Alexanderson, H., Ingólfsson, Ó., Murray, A. S., and Dudek, J. (2013). An interglacial polar bear and an early Weichselian glaciation at Poolepynten, western Svalbard. *Boreas* **42**, 532-543.
- Ankjærgaard, C., Jain, M., and Wallinga, J. (2013). Towards dating Quaternary sediments using the quartz Violet Stimulated Luminescence (VSL) signal. *Quaternary Geochronology* **18**, 99-109.
- Athanassas, C., and Fountoulis, I. (2013). Quaternary Neotectonic Configuration of the Southwestern Peloponnese, Greece, Based on Luminescence Ages of Marine Terraces. *Journal of Earth Science* **24**, 410-427.
- Avcioglu, M., Erginal, A. E., Kiyak, N. G., Kapan-Yeşilyurt, S., and Yiğitbaş, E. (2013). A preliminary note on depositional characteristics and optical luminescence age of a marine terrace, strait of Çanakkale, Turkey. *Journal of Coastal Research* **29**, 225-230.
- Avni, G., Porat, N., and Avni, Y. (2013). Byzantine-Early Islamic agricultural systems in the Negev Highlands: Stages of development as interpreted through OSL dating. *Journal of Field Archaeology* **38**, 332-346.
- Bailiff, I. K., Lewis, S. G., Drinkall, H. C., and White, M. J. (2013). Luminescence dating of sediments from a Palaeolithic site associated with a solution feature on the North Downs of Kent, UK. *Quaternary Geochronology* **18**, 135-148.
- Balescu, S. (2013). Chronology of Middle Pleistocene loess from Normandy. *Quaternaire* **24**, 237-245.
- Barros, L. F. D. P., and Junior, A. P. M. (2013). Quaternary alluvial sedimentation in the Conceição river valley, southeastern Brazil. *Brazilian Journal of Geology* **43**, 535-554.
- Bates, M., Pope, M., Shaw, A., Scott, B., and Schwenninger, J.-L. (2013). Late Neanderthal occupation in North-West Europe: rediscovery, investigation and dating of a last glacial sediment sequence at the site of La Cotte de Saint Brelade, Jersey. *Journal of Quaternary Science* **28**, 647-652.
- Berger, G. W., Doran, P. T., and Thomsen, K. J. (2013). Micro-hole and multigrain quartz luminescence dating of Paleodeltas at Lake Fryxell, McMurdo Dry Valleys (Antarctica), and relevance for lake history. *Quaternary Geochronology* **18**, 119-134.
- Biswas, R. H., Williams, M. A. J., Raj, R., Juyal, N., and Singhvi, A. K. (2013). Methodological studies on luminescence dating of volcanic ashes. *Quaternary Geochronology* **17**, 14-25.
- Bridgland, D. R., Harding, P., Allen, P., Candy, I., Cherry, C., George, W., Horne, D. J., Keen, D. H., Penkman, K. E. H., Preece, R. C., Rhodes, E. J., Scaife, R., Schreve, D. C., Schwenninger, J.-L., Slipper, I., Ward, G. R., White, M. J., White, T. S., and Whittaker, J. E. (2013). An enhanced record of MIS 9 environments, geochronology and geoarchaeology: data from construction of the High Speed 1 (London–Channel Tunnel) rail-link and other recent investigations at Purfleet, Essex, UK. *Proceedings of the Geologists' Association* **124**, 417-476.
- Buylaert, J. P., Murray, A. S., Gebhardt, A. C., Sohbati, R., Ohlendorf, C., Thiel, C., Wastegård, S., and Zolitschka, B. (2013). Luminescence dating of the PASADO core 5022-1D from Laguna Potrok Aike (Argentina) using IRSL signals from feldspar. *Quaternary Science Reviews* **71**, 70-80.
- Cano, N. F., Turbiani-Filho, I. T., Gennari, R. F., Munita, C. S., Souza, M. C., Angulo, R. J., and Watanabe, S. (2013). TL dating of sediments from Ilha do Mel, Brazil. *Quaternary International* **306**, 137-145.
- Chazan, M., Porat, N., Sumner, T. A., and Horwitz, L. K. (2013). The use of OSL dating in unstructured sands: The archaeology and chronology of the Hutton Sands at Canteen Kopje (Northern Cape Province, South Africa). *Archaeological and Anthropological Sciences* **5**, 351-363.
- Chen, L.-c., Ran, Y.-k., Wang, H., Shi, X., Liu, R.-c., and Dong, S.-p. (2013). Paleoseismology and kinematic characteristics of the Xiaoyudong rupture, a short but significant strange segment characterized by the May 12, 2008, Mw 7.9 earthquake in Sichuan, China. *Tectonophysics* **584**, 91-101.

- Chen, R., and Pagonis, V. (2013). Modeling TL-like thermally assisted optically stimulated luminescence (TA-OSL). *Radiation Measurements* **56**, 6-12.
- Chen, R., and Pagonis, V. (2013). On the expected order of kinetics in a series of thermoluminescence (TL) and thermally stimulated conductivity (TSC) peaks. *Nuclear Instruments and Methods in Physics Research Section B: Beam Interactions with Materials and Atoms* **312**, 60-69.
- Chen, Y., Zong, Y., Li, B., Li, S., and Aitchison, J. C. (2013). Shrinking lakes in Tibet linked to the weakening Asian monsoon in the past 8.2 ka. *Quaternary Research* **80**, 189-198.
- Choi, J.-H., Ryu, J.-S., Shin, H., Kim, J., and Cheong, C.-s. (2013). Reevaluation of Th and U concentrations in marine sediment reference materials using isotope dilution MC-ICP-MS: towards the analytical improvements in dose rate estimation for luminescence dating. *Geosciences Journal* **17**, 123-127.
- Chruścińska, A. (2013). Influence of spectral width of stimulation band on the shape of OSL curve. *Radiation Measurements* **56**, 18-22.
- Corcea, C. A., Constantin, D., Anechitei, V., Timar-Gabor, A., and Filipescu, S. (2013). SAR OSL dating of 63-90 μm quartz extracted from an Eemian (presumably lacustrine) sedimentary section at Florești on the Someșul Mic Valley. *Carpathian Journal of Earth and Environmental Sciences* **8**, 139-145.
- Corona, A., Perea, D., and McDonald, H. G. (2013). *Catonyx cuvieri* (Xenarthra, Mylodontidae, Scelidotheriinae) from the late Pleistocene of Uruguay, with comments regarding the systematics of the subfamily. *Journal of Vertebrate Paleontology* **33**, 1214-1225.
- Dawson, M.-C., Bernard-Guelle, S., Rué, M., and Fernandes, P. (2012). New data on the exploitation of flint outcrops during the Middle Palaeolithic: the Mousterian workshop of Chêne Vert at Dirac (Charente, France). *Paléo* **23**, 55-84.
- Dewar, R. E., Radimilahy, C., Wright, H. T., Jacobs, Z., Kelly, G. O., and Berna, F. (2013). Stone tools and foraging in northern Madagascar challenge Holocene extinction models. *Proceedings of the National Academy of Sciences* **110**, 12583-12588.
- Diana, R., Pasquale, B., Valentino, P., Federica, S., Rocco, P., Mariano, D., Donatella, B., and Antonino, O. (2013). SAR TL dating of Neolithic and Medieval ceramics from Lamezia, Calabria (South Italy): A case study. *Mediterranean Archaeology & Archaeometry* **13**, 277-288.
- Dreibrodt, S., Lubos, C., Hofmann, R., MÜLLER-Scheeßel, N., Richling, I., Nelle, O., Fuchs, M., Rassmann, K., Kujundžić-Vejzagić, Z., Bork, H. R., and MÜLLER, J. (2013). Holocene river and slope activity in the Visoko Basin, Bosnia-Herzegovina – climate and land-use effects. *Journal of Quaternary Science* **28**, 559-570.
- Duval, M., and Arnold, L. J. (2013). Field gamma dose-rate assessment in natural sedimentary contexts using LaBr₃(Ce) and NaI(Tl) probes: A comparison between the “threshold” and “windows” techniques. *Applied Radiation and Isotopes* **74**, 36-45.
- Fan, T., Fan, Y., Zhao, H., Chen, F., and Lai, Z. (2013). Investigations on the degree of bleaching of quartz OSL signals using modern aeolian dust from western Loess Plateau, China. *Geochronometria* **40**, 165-176.
- Fattahi, M., Karimi Moayed, N., Walker, R., and Talebian, M. (2013). Determining the slip rate on the Gowk fault using POST-IR method. *Journal of the Earth and Space Physics* **39**, 13-28.
- Fattahi, M., Walker, R. T., Talebian, M., Sloan, R. A., and Rasheedi, A. (2014). Late Quaternary active faulting and landscape evolution in relation to the Gowk Fault in the South Golbaf Basin, S.E. Iran. *Geomorphology* **204**, 334-343.
- Fiore, M., Soares, E. A. A., Mittani, J. C. R., Yee, M., and Tatumi, S. H. (2014). OSL dating of sediments from Negro and Solimões rivers – Amazon, Brazil. *Radiation Physics and Chemistry* **95**, 113-115.
- Fischer, P., Hilgers, A., Protze, J., Kels, H., Lehmkuhl, F., and Gerlach, R. (2012). Formation and geochronology of Last Interglacial to Lower Weichselian loess/palaeosol sequences – case studies from the Lower Rhine Embayment, Germany. *E&G Quaternary Science Journal* **61**, 48–63.
- Fitzsimmons, K. E., Hambach, U., Veres, D., and Iovita, R. (2013). The Campanian Ignimbrite Eruption: New Data on Volcanic Ash Dispersal and Its Potential Impact on Human Evolution. *PLoS ONE* **8**, e65839.

- Fraser, J. A., and Price, D. M. (2013). A thermoluminescence (TL) analysis of ceramics from cairns in Jordan: Using TL to integrate off-site features into regional chronologies. *Applied Clay Science* **82**, 24-30.
- Fu, X., and Li, S.-H. (2013). A modified multi-elevated-temperature post-IR IRSL protocol for dating Holocene sediments using K-feldspar. *Quaternary Geochronology* **17**, 44-54.
- Fuchs, M., Kreutzer, S., Rousseau, D.-D., Antoine, P., Hatté, C., Lagroix, F., Moine, O., Gauthier, C., Svoboda, J., and Lisá, L. (2013). The loess sequence of Dolní Věstonice, Czech Republic: A new OSL-based chronology of the Last Climatic Cycle. *Boreas* **42**, 664-677.
- Fuchs, M. C., Böhlert, R., Krbetschek, M., Preusser, F., and Egli, M. (2013). Exploring the potential of luminescence methods for dating Alpine rock glaciers. *Quaternary Geochronology* **18**, 17-33.
- Gong, Z., Li, S.-H., Sun, J., and Xue, L. (2013). Environmental changes in Hunshandake (Otindag) sandy land revealed by optical dating and multi-proxy study of dune sands. *Journal of Asian Earth Sciences* **76**, 30-36.
- Hanebuth, T. J. J., Kudrass, H. R., Linstädter, J., Islam, B., and Zander, A. M. (2013). Rapid coastal subsidence in the central Ganges-Brahmaputra Delta (Bangladesh) since the 17th century deduced from submerged salt-producing kilns. *Geology* **41**, 987-990.
- Hedrick, K., Owen, L. A., Rockwell, T. K., Meigs, A., Costa, C., Caffee, M. W., Masana, E., and Ahumada, E. (2013). Timing and nature of alluvial fan and strath terrace formation in the Eastern Precordillera of Argentina. *Quaternary Science Reviews* **80**, 143-168.
- Hernandez, M., Mercier, N., Bertran, P., Colonge, D., and Lelouvier, L. A. (2012). First dating results for the Middle Pleistocene industries (Acheulean – Early Middle Palaeolithic) in the Pyrenees – Garonne region: a multi methods geochronological approach (TL, OSL and TT-OSL) of the Duclos and Romentères sites. *Paléo* **23**, 155-170.
- Hipondoka, M. H. T., Mauz, B., Kempf, J., Packman, S., Chiverrell, R. C., and Bloemendal, J. (2014). Chronology of sand ridges and the Late Quaternary evolution of the Etosha Pan, Namibia. *Geomorphology* **204**, 553-563.
- Houben, P., Köhl, N., Dambeck, R., and Overath, J. (2013). Lateglacial to Holocene rapid crater infilling of a MIS 2 maar volcano (West-Eifel Volcanic Field, Germany): environmental history and geomorphological feedback mechanisms. *Boreas* **42**, 947-958.
- Huang, C. C., Pang, J., Zhou, Y., Su, H., Zhang, Y., and Wang, L. (2013). Palaeoenvironmental implications of the prehistorical catastrophes in relation to the Lajia Ruins within the Guanting Basin along the Upper Yellow River, China. *The Holocene* **23**, 1584-1595.
- Jiang, H., Mao, X., Xu, H., Yang, H., Ma, X., Zhong, N., and Li, Y. (2014). Provenance and earthquake signature of the last deglacial Xinmocun lacustrine sediments at Diexi, East Tibet. *Geomorphology* **204**, 518-531.
- Kang, S., Wang, X., and Lu, Y. (2013). Quartz OSL chronology and dust accumulation rate changes since the Last Glacial at Weinan on the southeastern Chinese Loess Plateau. *Boreas* **42**, 815-829.
- Karabacak, V., Yönlü, Ö., Dökü, E., Kiyak, N. G., Altunel, E., Özüdoğru, Ş., Yalçiner, C. Ç., and Akyüz, H. S. (2013). Analyses of Seismic Deformation at the Kibyra Roman Stadium, Southwest Turkey. *Geoarchaeology* **28**, 531-543.
- Kehl, M., Burow, C., Hilgers, A., Navazo, M., Pastoors, A., Weniger, G.-C., Wood, R., and Jordá Pardo, J. F. (2013). Late Neanderthals at Jarama VI (central Iberia)? *Quaternary Research* **80**, 218-234.
- Kermode, S. J., Gibling, M. R., Jones, B. G., Cohen, T. J., Price, D. M., and Daley, J. S. (2013). Determining the impact of the Holocene highstand at the coastal-fluvial interface, Shoalhaven River, south-eastern Australia. *Earth Surface Processes and Landforms* **38**, 1481-1495.
- Kijek, N., Chruścińska, A., and Przegiętka, K. R. (2013). On the dependence of equivalent dose on temperature of OSL measurements for sediment quartz grains and its implication in dating practice. *Radiation Measurements* **56**, 252-256.
- King, G. E., Robinson, R. A. J., and Finch, A. A. (2013). Apparent OSL ages of modern deposits from Fåbergstølsdalen, Norway: implications for sampling glacial sediments. *Journal of Quaternary Science* **28**, 673-682.

- Kinnaird, T., and Robertson, A. (2013). Tectonic and sedimentary response to subduction and incipient continental collision in southern cyprus, easternmost mediterranean region. *Geological Society Special Publication* **372**, 585-614.
- Kiss, T., Sümeghy, B., and Sipos, G. (2014). Late Quaternary paleodrainage reconstruction of the Maros River alluvial fan. *Geomorphology* **204**, 49-60.
- Klasen, N., Hilgers, A., Schmidt, C., Bertrams, M., Schyle, D., Lehmkuhl, F., Richter, J., and Radtke, U. (2013). Optical dating of sediments in Wadi Sabra (SW Jordan). *Quaternary Geochronology* **18**, 9-16.
- Kliem, P., Buylaert, J. P., Hahn, A., Mayr, C., Murray, A. S., Ohlendorf, C., Veres, D., Wastegård, S., and Zolitschka, B. (2013). Magnitude, geomorphologic response and climate links of lake level oscillations at Laguna Potrok Aike, Patagonian steppe (Argentina). *Quaternary Science Reviews* **71**, 131-146.
- Kuerten, S., Parolin, M., Assine, M. L., and McGlue, M. M. (2013). Sponge spicules indicate Holocene environmental changes on the Nabileque River floodplain, southern Pantanal, Brazil. *Journal of Paleolimnology* **49**, 171-183.
- Kuneš, P., Kjærsgaard Sørensen, M., Buylaert, J.-P., Murray, A. S., Houmark-Nielsen, M., and Odgaard, B. V. (2013). A new Middle Pleistocene interglacial record from Denmark: Chronostratigraphic correlation, palaeovegetation and fire dynamics. *Boreas* **42**, 596-612.
- Lacelle, D., Davila, A. F., Fisher, D., Pollard, W. H., DeWitt, R., Heldmann, J., Marinova, M. M., and McKay, C. P. (2013). Excess ground ice of condensation–diffusion origin in University Valley, Dry Valleys of Antarctica: Evidence from isotope geochemistry and numerical modeling. *Geochimica et Cosmochimica Acta* **120**, 280-297.
- Lail, W., Sammeth, D., Mahan, S., and Nevins, J. (2013). A Non-Destructive Method for Dating Human Remains. *Advances in Archaeological Practice* **1**, 91-103.
- Langgut, D., Gadot, Y., Porat, N., and Lipschits, O. (2013). Fossil pollen reveals the secrets of the Royal Persian Garden at Ramat Rahel, Jerusalem. *Palynology* **37**, 115-129.
- Larsen, A., Bork, H.-R., Fuelling, A., Fuchs, M., and Larsen, J. R. (2013). The processes and timing of sediment delivery from headwaters to the trunk stream of a Central European mountain gully catchment. *Geomorphology* **201**, 215-226.
- Leighton, C. L., Bailey, R. M., and Thomas, D. S. G. (2013). The utility of desert sand dunes as Quaternary chronostratigraphic archives: evidence from the northeast Rub' al Khali. *Quaternary Science Reviews* **78**, 303-318.
- Lemdahl, G., Broström, A., HedenÄS, L., Arvidsson, K., Holmgren, S., Gaillard, M.-J., and MÖLLer, P. E. R. (2013). Eemian and Early Weichselian environments in southern Sweden: a multi-proxy study of till-covered organic deposits from the Småland peneplain. *Journal of Quaternary Science* **28**, 705-719.
- Lepper, K., Buell, A. W., Fisher, T. G., and Lowell, T. V. (2013). A chronology for glacial Lake Agassiz shorelines along Upham's namesake transect. *Quaternary Research* **80**, 88-98.
- Li, B., Jacobs, Z., Roberts, R. G., and Li, S.-H. (2013). Extending the age limit of luminescence dating using the dose-dependent sensitivity of MET-pIRIR signals from K-feldspar. *Quaternary Geochronology* **17**, 55-67.
- Li, B., Roberts, R. G., and Jacobs, Z. (2013). On the dose dependency of the bleachable and non-bleachable components of IRSL from K-feldspar: Improved procedures for luminescence dating of Quaternary sediments. *Quaternary Geochronology* **17**, 1-13.
- Litwin, R. J., Smoot, J. P., Pavich, M. J., Markewich, H. W., Brook, G., and Durika, N. J. (2013). 100,000-year-long terrestrial record of millennial-scale linkage between eastern North American mid-latitude paleovegetation shifts and Greenland ice-core oxygen isotope trends. *Quaternary Research* **80**, 291-315.
- Liu, D., Chen, G., Lai, Z., Weis, H., Zhou, G., and Peng, M. (2013). Late Glacial and Holocene vegetation and climate history of an alpine wetland on the Qinghai-Tibetan Plateau. *Geological Quarterly* **57**, 261–268.
- Lyons, R., Tooth, S., and Duller, G. A. T. (2013). Chronology and controls of donga (gully) formation in the upper Blood River catchment, KwaZulu-Natal, South Africa: Evidence for a climatic driver of erosion. *The Holocene* **23**, 1875-1887.

- Madole, R. F., Mahan, S. A., Romig, J. H., and Havens, J. C. (2013). Constraints on the age of the Great Sand Dunes, Colorado, from subsurface stratigraphy and OSL dates. *Quaternary Research* **80**, 435-446.
- Meier, H. A., Nordt, L. C., Forman, S. L., and Driese, S. G. (2013). Late Quaternary alluvial history of the middle Owl Creek drainage basin in central Texas: A record of geomorphic response to environmental change. *Quaternary International* **306**, 24-41.
- Mercier, N., Valladas, H., Falguères, C., Shao, Q., Gopher, A., Barkai, R., Bahain, J.-J., Vialettes, L., Joron, J.-L., and Reyss, J.-L. (2013). New datings of Amudian layers at Qesem Cave (Israel): results of TL applied to burnt flints and ESR/U-series to teeth. *Journal of Archaeological Science* **40**, 3011-3020.
- Meyer, M. C., Austin, P., and Tropper, P. (2013). Quantitative evaluation of mineral grains using automated SEM–EDS analysis and its application potential in optically stimulated luminescence dating. *Radiation Measurements* **58**, 1-11.
- Mishra, S., Chauhan, N., and Singhvi, A. K. (2013). Continuity of Microblade Technology in the Indian Subcontinent Since 45 ka: Implications for the Dispersal of Modern Humans. *PLoS ONE* **8**, e69280.
- Muhs, D. R., Bettis III, E. A., Roberts, H. M., Harlan, S. S., Paces, J. B., and Reynolds, R. L. (2013). Chronology and provenance of last-glacial (Peoria) loess in western Iowa and paleoclimatic implications. *Quaternary Research* **80**, 468-481.
- Muñoz-Salinas, E., Castillo, M., Sanderson, D., and Kinnaird, T. (2013). Unraveling paraglacial activity on Sierra de Gredos, Central Spain: A study based on geomorphic markers, stratigraphy and OSL. *Catena* **110**, 207-214.
- Nawaz Ali, S., Biswas, R. H., Shukla, A. D., and Juyal, N. (2013). Chronology and climatic implications of Late Quaternary glaciations in the Goriganga valley, central Himalaya, India. *Quaternary Science Reviews* **73**, 59-76.
- Necea, D., Fielitz, W., Kadereit, A., Andriessen, P. A. M., and Dinu, C. (2013). Middle Pleistocene to Holocene fluvial terrace development and uplift-driven valley incision in the SE Carpathians, Romania. *Tectonophysics* **602**, 332-354.
- Ninis, D., Little, T. A., Van Dissen, R. J., Litchfield, N. J., Smith, E. G. C., Wang, N., Rieser, U., and Henderson, C. M. (2013). Slip rate on the wellington fault, New Zealand, during the late quaternary: Evidence for variable slip during the Holocene. *Bulletin of the Seismological Society of America* **103**, 559-579.
- Ortega, B., Schaaf, P., Murray, A.S., Caballero, M., Lozano, S., and Ramirez, A. (2013). Eolian deposition cycles since AD 500 in Playa San Bartolo lunette dune, Sonora, Mexico: Paleoclimatic implications. *Aeolian Research* **11**, 1-13.
- Pagonis, V., Chithambo, M. L., Chen, R., Chruścińska, A., Fasoli, M., Li, S. H., Martini, M., and Ramseyer, K. (2014). Thermal dependence of luminescence lifetimes and radioluminescence in quartz. *Journal of Luminescence* **145**, 38-48.
- Panzeri, L. (2013). Mortar and surface dating with optically stimulated luminescence (OSL): Innovative techniques for the age determination of buildings. *Nuovo Cimento della Società Italiana di Fisica C* **36**, 205-216.
- Pappalardo, M., Chelli, A., Ciampalini, A., Rellini, I., Biagioni, F., Brückner, H., Fülling, A., and Firpo, M. (2013). Evolution of an Upper Pleistocene aeolianite in the northern Mediterranean (Liguria, NW Italy). *Italian Journal of Geosciences* **132**, 290-303.
- Parham, P. R., Riggs, S. R., Culver, S. J., Mallinson, D. J., Rink, W. J., and Burdette, K. (2013). Quaternary coastal lithofacies, sequence development and stratigraphy in a passive margin setting, North Carolina and Virginia, USA. *Sedimentology* **60**, 503-547.
- Pederson, J., Burnside, N., Shipton, Z., and Rittenour, T. (2013). Rapid river incision across an inactive fault—Implications for patterns of erosion and deformation in the central Colorado Plateau. *Lithosphere* **5**, 513-520.
- Pesce, G. L., Micheletto, E., Quarta, G., Uggè, S., Calcagnile, L., and Decri, A. (2013). Radiocarbon dating of mortars from the baptismal font of the San Lorenzo cathedral of Alba (cuneo, Italy): Comparison with thermoluminescence dating of related bricks and pipes. *Radiocarbon* **55**, 526-533.
- Plotzki, A., May, J. H., Preusser, F., and Veit, H. (2013). Geomorphological and sedimentary evidence for late Pleistocene to Holocene hydrological change along the Río Mamoré, Bolivian Amazon. *Journal of South American Earth Sciences* **47**, 230-242.

- Przegiętka, K. R., and Chruścińska, A. (2013). Analysis of optical bleaching of OSL signal in sediment quartz. *Radiation Measurements* **56**, 257-261.
- Reddy, D. V., Singaraju, V., Mishra, R., Kumar, D., Thomas, P. J., Rao, K. K., and Singhvi, A. K. (2013). Luminescence chronology of the inland sand dunes from SE India. *Quaternary Research* **80**, 265-273.
- Ren, J., Xu, X., Yeats, R. S., and Zhang, S. (2013). Latest Quaternary paleoseismology and slip rates of the Longriba fault zone, eastern Tibet: Implications for fault behavior and strain partitioning. *Tectonics* **32**, 216-238.
- Ren, J., Xu, X., Yeats, R. S., and Zhang, S. (2013). Millennial slip rates of the Tazang fault, the eastern termination of Kunlun fault: Implications for strain partitioning in eastern Tibet. *Tectonophysics* **608**, 1180-1200.
- Rink, W. J., Mercier, N., Mihailovic, D., Morley, M. W., Thompson, J. W., and Roksandic, M. (2013). New Radiometric Ages for the BH-1 Hominin from Balanica (Serbia): Implications for Understanding the Role of the Balkans in Middle Pleistocene Human Evolution. *Plos One* **8**.
- Ristuccia, G. M., Di Stefano, A., Gueli, A. M., Monaco, C., Stella, G., and Troja, S. O. (2013). OSL chronology of Quaternary terraced deposits outcropping between Mt. Etna volcano and the Catania Plain (Sicily, southern Italy). *Physics and Chemistry of the Earth, Parts A/B/C* **63**, 36-46.
- Roqué, C., Linares, R., Zarroca, M., Rosell, J., Pellicer, X. M., and Gutiérrez, F. (2013). Chronology and paleoenvironmental interpretation of talus flatiron sequences in a sub-humid mountainous area: Tremp Depression, Spanish Pyrenees. *Earth Surface Processes and Landforms* **38**, 1513-1522.
- Roskin, J., Katra, I., Porat, N., and Zilberman, E. (2013). Evolution of Middle to Late Pleistocene sandy calcareous paleosols underlying the northwestern Negev Desert Dunefield (Israel). *Palaeogeography, Palaeoclimatology, Palaeoecology* **387**, 134-152.
- Schmidt, C., Sitlivy, V., Anghelinu, M., Chabai, V., Kels, H., Uthmeier, T., Hauck, T., Bălțean, I., Hilgers, A., Richter, J., and Radtke, U. (2013). First chronometric dates (TL and OSL) for the Aurignacian open-air site of Românești-Dumbrăvița I, Romania. *Journal of Archaeological Science* **40**, 3740-3753.
- Simkins, L. M., Simms, A. R., and DeWitt, R. (2013). Relative sea-level history of Marguerite Bay, Antarctic Peninsula derived from optically stimulated luminescence-dated beach cobbles. *Quaternary Science Reviews* **77**, 141-155.
- Simms, A. R., Anderson, J. B., DeWitt, R., Lambeck, K., and Purcell, A. (2013). Quantifying rates of coastal subsidence since the last interglacial and the role of sediment loading. *Global and Planetary Change* **111**, 296-308.
- Simón, J. L., Pérez-Cueva, A. J., and Calvo-Cases, A. (2013). Tectonic beheading of fluvial valleys in the Maestrat grabens (eastern Spain): Insights into slip rates of Pleistocene extensional faults. *Tectonophysics* **593**, 73-84.
- Soressi, M., McPherron, S. P., Lenoir, M., Dogandžić, T., Goldberg, P., Jacobs, Z., Maigrot, Y., Martisius, N. L., Miller, C. E., Rendu, W., Richards, M., Skinner, M. M., Steele, T. E., Talamo, S., and Texier, J.-P. (2013). Neandertals made the first specialized bone tools in Europe. *Proceedings of the National Academy of Sciences* **110**, 14186-14190.
- Spiske, M., Piepenbreier, J., Benavente, C., Kunz, A., Bahlburg, H., and Steffahn, J. (2013). Historical tsunami deposits in Peru: Sedimentology, inverse modeling and optically stimulated luminescence dating. *Quaternary International* **305**, 31-44.
- Srivastava, P., Kumar, A., Mishra, A., Meena, N. K., Tripathi, J. K., Sundriyal, Y. P., Agnihotri, R., and Gupta, A. K. (2013). Early Holocene monsoonal fluctuations in the Garhwal higher Himalaya as inferred from multi-proxy data from the Malari paleolake. *Quaternary Research* **80**, 447-458.
- Srivastava, P., Ray, Y., Phartiyal, B., and Sharma, A. (2013). Late Pleistocene-Holocene morphosedimentary architecture, Spiti River, arid higher Himalaya. *International Journal of Earth Sciences* **102**, 1967-1984.
- Stamm, J. F., Hendricks, R. R., Sawyer, J. F., Mahan, S. A., Zaprowski, B. J., Geibel, N. M., and Azzolini, D. C. (2013). Late Quaternary stream piracy and strath terrace formation along the Belle Fourche and lower Cheyenne Rivers, South Dakota and Wyoming. *Geomorphology* **197**, 10-20.
- Starnberger, R., Rodnight, H., and Spötl, C. (2013). Luminescence dating of fine-grain lacustrine sediments from the late Pleistocene Unterangerberg site (Tyrol, Austria). *Austrian Journal of Earth Sciences* **106**, 4-15.

- Stella, G., Fontana, D., Gueli, A., and Troja, S. (2013). Historical mortars dating from OSL signals of fine grain fraction enriched in quartz. *Geochronometria* **40**, 153-164.
- Stevens, T., Adamiec, G., Bird, A. F., and Lu, H. (2013). An abrupt shift in dust source on the Chinese Loess Plateau revealed through high sampling resolution OSL dating. *Quaternary Science Reviews* **82**, 121-132.
- Swezey, C. S., Schultz, A. P., González, W. A., Bernhardt, C. E., Doar Iii, W. R., Garrity, C. P., Mahan, S. A., and McGeehin, J. P. (2013). Quaternary eolian dunes in the Savannah River valley, Jasper County, South Carolina, USA. *Quaternary Research* **80**, 250-264.
- Timar-Gabor, A., and Wintle, A. G. (2013). On natural and laboratory generated dose response curves for quartz of different grain sizes from Romanian loess. *Quaternary Geochronology* **18**, 34-40.
- Tooth, S., McCarthy, T., Rodnight, H., Keen-Zebert, A., Rowberry, M., and Brandt, D. (2014). Late Holocene development of a major fluvial discontinuity in floodplain wetlands of the Blood River, eastern South Africa. *Geomorphology* **205**, 128-141.
- Tribolo, C., Mercier, N., Douville, E., Joron, J. L., Reyss, J. L., Rufer, D., Cantin, N., Lefrais, Y., Miller, C. E., Porraz, G., Parkington, J., Rigaud, J. P., and Texier, P. J. (2013). OSL and TL dating of the Middle Stone Age sequence at Diepkloof Rock Shelter (South Africa): a clarification. *Journal of Archaeological Science* **40**, 3401-3411.
- Trindade, M. J., Prudencio, M. I., Sanjurjo-Sanchez, J., Romani, J. R. V., Ferraz, T., Fernandez Mosquera, D., and Dias, M. I. (2013). Post-depositional processes of elemental enrichment inside dark nodular masses of an ancient aeolian dune from A Coruna, Northwest Spain. *Geologica Acta* **11**, 231-244.
- Tripaldi, A., Zárate, M. A., Forman, S. L., Badger, T., Doyle, M. E., and Cicciooli, P. (2013). Geological evidence for a drought episode in the western Pampas (Argentina, South America) during the early-mid 20th century. *The Holocene* **23**, 1731-1746.
- van Gorp, W., Veldkamp, A., Temme, A. J. A. M., Maddy, D., Demir, T., van der Schriek, T., Reimann, T., Wallinga, J., Wijbrans, J., and Schoorl, J. M. (2013). Fluvial response to Holocene volcanic damming and breaching in the Gediz and Geren rivers, western Turkey. *Geomorphology* **201**, 430-448.
- Wacha, L., Galović, L., Koloszár, L., Magyari, A., Chikán, G., and Marsi, I. (2013). The chronology of the Šarengrad II loess-palaeosol section (Eastern Croatia). *Geologia Croatica* **66**, 191-203.
- Wallinga, J., van Mourik, J. M., and Schilder, M. L. M. (2013). Identifying and dating buried micropodzols in Subatlantic polycyclic drift sands. *Quaternary International* **306**, 60-70.
- Wang, X., Vandenberghe, D., Yi, S., Vandenberghe, J., Lu, H., Van Balen, R., and Van den Haute, P. (2013). Late Quaternary paleoclimatic and geomorphological evolution at the interface between the Menyuan basin and the Qilian Mountains, northeastern Tibetan Plateau. *Quaternary Research* **80**, 534-544.
- Weckwerth, P., Przegietka, K. R., Chruscinska, A., and Pisarska-Jamrozy, M. (2013). The relation between optical bleaching and sedimentological features of fluvial deposits in the Torun Basin (Poland). *Geological Quarterly* **57**, 31-44.
- Westaway, M. C., Cupper, M. L., Johnston, H., and Graham, I. (2013). The Willandra Fossil Trackway: Assessment of ground penetrating radar survey results and additional OSL dating at a unique Australian site. *Australian Archaeology* **76**, 84-89.
- Whitfield, R. G., Macklin, M. G., Brewer, P. A., Lang, A., Mauz, B., and Whitfield, E. (2013). The nature, timing and controls of the Quaternary development of the Rio Bergantes, Ebro basin, northeast Spain. *Geomorphology* **196**, 106-121.
- Williams, A. N., Mitchell, P., Wright, R. V. S., and Toms, P. S. (2013). A terminal Pleistocene open site on the Hawkesbury River, Pitt town, New South Wales. *Australian Archaeology* **74**, 85-97.
- Williams, G. E., Gostin, V. A., and Prescott, J. R. (2013). Stratigraphy and optical dating of Pleistocene coastal deposits in the Port Campbell australite strewn field, SW Victoria. *Australian Journal of Earth Sciences* **60**, 463-474.
- Wróblewski, R., Fedorowicz, S., and Kamińska, K. (2013). Holocene sediments of the Ustka Cliff (Northern Poland) in view of radiometric dating. *Geochronometria* **40**, 187-194.

Yang, X., Wang, X., Liu, Z., Li, H., Ren, X., Zhang, D., Ma, Z., Rioual, P., Jin, X., and Scuderi, L. (2013). Initiation and variation of the dune fields in semi-arid China – with a special reference to the Hunshandake Sandy Land, Inner Mongolia. *Quaternary Science Reviews* **78**, 369-380.

Yildirim, C., Melnick, D., Ballato, P., Schildgen, T. F., Echtler, H., Erginal, A. E., K1yak, N. G., and Strecker, M. R. (2013). Differential uplift along the northern margin of the Central Anatolian Plateau: inferences from marine terraces. *Quaternary Science Reviews* **81**, 12-28.

Zhang, J., and Cunningham, D. (2013). Polyphase transpressional development of a NNE-striking basement-cored anticline in the Xining Basin, northeastern Qinghai-Tibetan Plateau. *Geological Magazine* **150**, 626-638.

Zhang, Y., Huang, C. C., Pang, J., Zha, X., Zhou, Y., and Gu, H. (2013). Holocene paleofloods related to climatic events in the upper reaches of the Hanjiang River valley, middle Yangtze River basin, China. *Geomorphology* **195**, 1-12.

Zhao, J., Yin, X., Harbor, J. M., Lai, Z., Liu, S., and Li, Z. (2013). Quaternary glacial chronology of the Kanas River valley, Altai Mountains, China. *Quaternary International* **311**, 44-53.

Zheng, W. J., Zhang, P. Z., Ge, W. P., Molnar, P., Zhang, H. P., Yuan, D. Y., and Liu, J. H. (2013). Late Quaternary slip rate of the South Heli Shan Fault (northern Hexi Corridor, NW China) and its implications for northeastward growth of the Tibetan Plateau. *Tectonics* **32**, 271-293.

Zular, A., Sawakuchi, A. O., Guedes, C. C. F., Mendes, V. R., Nascimento, D. R., Jr., Giannini, P. C. F., Aguiar, V. A. P., and DeWitt, R. (2013). Late Holocene intensification of colds fronts in southern Brazil as indicated by dune development and provenance changes in the Sao Francisco do Sul coastal barrier. *Marine Geology* **335**, 64-77.

Papers from the 3rd Asia Pacific LED 2012, published in *Geochronometria* 40/4

Alappat, L., Seralathan, P., Shukla, A., Thrivikramji, K., and Singhvi, A. (2013). Chronology of red dune aggradations of South India and its Palaeo-environmental significance. *Geochronometria* **40**, 274-282.

Biswas, R., and Singhvi, A. (2013). Anomalous fading and crystalline structure: Studies on individual chondrules from the same parent body. *Geochronometria* **40**, 250-257.

Chen, Y., Li, S.-H., and Li, B. (2013). Residual doses and sensitivity change of post IR IRSL signals from potassium feldspar under different bleaching conditions. *Geochronometria* **40**, 229-238.

De Sarkar, S., Mathew, G., Pande, K., Chauhan, N., and Singhvi, A. (2013). Rapid denudation of Higher Himalaya during late Pleistocene, evidence from OSL thermochronology. *Geochronometria* **40**, 304-310.

Joannes-Boyau, R. (2013). Detailed protocol for an accurate non-destructive direct dating of tooth enamel fragment using Electron Spin Resonance. *Geochronometria* **40**, 322-333.

Kayama, M., Nishido, H., Toyoda, S., Komuro, K., Finch, A., Lee, M., and Ninagawa, K. (2013). Response of cathodoluminescence of alkali feldspar to He⁺ ion implantation and electron irradiation. *Geochronometria* **40**, 244-249.

Liu, C.-R., Yin, G.-M., Fang, F., Voinchet, P., Deng, C.-L., Han, F., Li, J.-P., Song, W.-J., Wang, D., and Bahain, J.-J. (2013). ESR dating of the Donggutuo Palaeolithic site in the Nihewan Basin, northern China. *Geochronometria* **40**, 348-354.

Nishido, H., Endo, T., Ninagawa, K., Kayama, M., and Gucsik, A. (2013). Thermal effects on cathodoluminescence in forsterite. *Geochronometria* **40**, 239-243.

Richter, D., Richter, A., and Dornich, K. (2013). lexsyg - a new system for luminescence research. *Geochronometria* **40**, 220-228.

Schielein, P., and Lomax, J. (2013). The effect of fluvial environments on sediment bleaching and Holocene luminescence ages — A case study from the German Alpine Foreland. *Geochronometria* **40**, 283-293.

- Shimada, A., Takada, M., and Toyoda, S. (2013). Characteristics of ESR signals and TLCLs of quartz included in various source rocks and sediments in Japan: A clue to sediment provenance. *Geochronometria* **40**, 334-340.
- Shitaoka, Y., and Nagatomo, T. (2013). OSL dating using quartz fine grains extracted from loess in Upper Palaeolithic sites of Nihewan Basin, northern China. *Geochronometria* **40**, 311-316.
- Soni, A., Mishra, D., Bhatt, B., Gupta, S., Rawat, N., Kulkarni, M., and Sharma, D. (2013). Thermally assisted OSL: A potent tool for improvement in minimum detectable dose and extension of dose range of Al₂O₃:C. *Geochronometria* **40**, 258-265.
- Tsukamoto, S., Kataoka, K., and Miyabuchi, Y. (2013). Luminescence dating of volcanogenic outburst flood sediments from Aso volcano and tephric loess deposits, southwest Japan. *Geochronometria* **40**, 294-303.
- Varma, V., Biswas, R., and Singhvi, A. (2013). Aspects of Infrared Radioluminescence dosimetry in K-feldspar. *Geochronometria* **40**, 266-273.
- Voinchet, P., Yin, G., Falguères, C., Liu, C., Han, F., Sun, X., and Bahain, J. (2013). ESR dose response of Al center measured in quartz samples from the Yellow River (China): Implications for the dating of Upper Pleistocene sediment. *Geochronometria* **40**, 341-347.
- Wu, Y., Jin, Z., Fan, A., and Fang, H. (2013). Firing temperature of a clay core sample in a bronze tripod from Daxinzhuang Site in China using TL techniques. *Geochronometria* **40**, 317-321.
- Yamamoto, Y., Toyoda, S., Nagasima, K., Igarashi, Y., and Tada, R. (2013). Investigation of the temporal change of the sources of Aeolian dust delivered to East Asia using electron spin resonance signals in quartz. *Geochronometria* **40**, 355-359.

Conference Announcements

LumiDoz 8

International Conference on Luminescence and ESR Dosimetry

August 27 – 29, 2014

Institute of Nuclear Sciences, Ankara University (Turkey) is inviting you to participate to International Conference on Luminescence and ESR Dosimetry (LumiDoz 8).

The conference will take place at the Institute of Nuclear Sciences, Ankara University, in Ankara-Turkey, between 27th and 29th August 2014.

The conference hopes to attract researchers with fundamental and applied research presentations covering luminescence mechanisms, new luminescent materials, applied radiation physics, dosimetry, detection of irradiated foods, archaeological and geological dating and other related issues and technological applications. The conference is bilingual, both English and Turkish contributions are welcome.

Proceedings of both oral and poster presentations – those eligible for peer-reviewed publication- will be published in Journal of Nuclear Science (limited to one first-author paper per active participant).

The web page of the conference is <http://lumidoz.en.ankara.edu.tr/>. You may find detailed information about registration, accommodation and deadlines here. You can also reach us by email at lumidoz@ankara.edu.tr.

On behalf of the Organising Committee of Lumidoz8.

Submission of articles to Ancient TL

Reviewing System

In order to ensure acceptable standards and minimize delay in publication, a modification of the conventional refereeing system has been devised for Ancient TL:

Articles can be sent directly by authors to a member of the Reviewers Panel chosen on the basis of the subject matter, but who is not in any of the authors' laboratories. **At the discretion of the Editor**, reviewers who are not listed in the Panel may be used.

The reviewing system aims to encourage direct dialogue between author and reviewer. The Editor should be kept advised of the progress of articles under review by sending him copies of all correspondence. He is available for advice where reviewing difficulties have arisen. Authors whose mother tongue is not English are required to have their manuscript revised for English *before* submitting it.

We ask reviewers to specify (where required) the minimum of revision that is consistent with achieving a clear explanation of the subject of the paper, the emphasis being on *rapid* publication; reviewers are encouraged to make a brief written comment for publication at the end of the paper. Where a contribution is judged not to meet an adequate standard without substantial modification, the author will be advised that the contribution is not suitable for publication. Articles that are not considered to be of sufficient interest may also be rejected.

Procedures

1. Articles should be submitted to an appropriate member of the Reviewing Panel or Editorial Board, chosen on the basis of the subject matter, but who is not in any of the authors' laboratories.
2. Articles should not normally exceed the equivalent of 5000 words inclusive of diagrams, tables and references. Greater space will be appropriate for certain topics; for these the Editor should first be consulted.
Short notes and letters are also invited. These should not exceed two printed pages in Ancient TL, including diagrams, tables and references (equivalent to ~1400 words of text).
3. Diagrams and labels should be ready for direct reproduction and not normally exceed 12 cm wide by 10 cm high. Where possible, high quality electronic versions of figures should be submitted. Separate figure captions should be supplied. Inappropriately scaled drawings and labels will be returned for alteration.
4. Authors are asked to submit the paper, including diagrams, to the Reviewer and a duplicate copy to the Editor.
The final version of the text must be submitted to the Editor electronically using a standard format (Microsoft Word for PC is currently used for producing Ancient TL). Electronic copies of Diagrams and Tables should also be submitted.
5. Upon receipt of an article, the Editor will send an acknowledgement to the author. If the Reviewer is unable to deal with the contribution within **4 weeks** he/she will inform the author and advise the Editor.

Requirements under various situations

When agreement concerning an article has been reached:

The Editor should receive a copy of the final version of the paper, both as hard copy and electronically. The Reviewer should send their final decision, including comments for publication if any, to the Editor.

If the article has not been rejected, but agreement on its final form cannot be reached or where there are protracted delays in the reviewing process:

The Editor may request an assessment from the Reviewer and responsibility passes to the Editor.

If the article is rejected:

The Editor and author receive notification from the Reviewer, with an indication of the reason for rejection.

Thesis abstracts are to be sent to the Editor and in principle do not need reviewing. However, authors are requested to make sure that the English is correct before submission. Thesis abstracts should not exceed 750 words, and figures and tables are not accepted.

Advertising. Formal information on equipment can be published in Ancient TL. It should not exceed one printed page. Current charges are displayed on the website (<http://www.aber.ac.uk/ancient-tl>)

Subscriptions to Ancient TL

Ancient TL is published 2 times a year and is sent Airmail to subscribers outside the United Kingdom. While every attempt will be made to keep to publication schedule, the Editorial Board may need to alter the number and frequency of issues, depending on the number of available articles which have been accepted by reviewers.

The subscription rate for 2014 is £15 for individual subscribers and £25 for Institutional subscription, plus any taxes where required. Payment must be in pounds sterling. Enquiries and orders must be sent to the Editor. Payment may be by cheques, made payable to 'Aberystwyth University', by credit/debit cards or by bank transfers. Further information on subscriptions is available on the Ancient TL web site (<http://www.aber.ac.uk/ancient-tl>)